3D Printed Gelatin/PTMC Core/Shell Scaffolds with NIR Laser-Tuned Drug/Biomolecule Release for Cancer Therapy and Uterine Regeneration

Shangsi Chen [a], Jiahui Lai [a], Jizhuo Chen [a], Liwu Zheng [b], Min Wang [a, *]

[a] Department of Mechanical Engineering

The University of Hong Kong

Pokfulam Road, Hong Kong SAR, China

[b] Faculty of Dentistry

The University of Hong Kong

34 Hospital Road, Sai Ying Pun, Hong Kong SAR, China

Keywords: 3D printing, core/shell scaffolds, cancer therapy, uterine regeneration, dual release

---

* Corresponding Author:

Professor Min Wang, at the University of Hong Kong, Hong Kong, China

Email: memwang@hku.hk Tel: +852 3971 7903 Fax: +852 2858541

Abstract

Surgical resection is an efficient treatment for cancerous tissues and uterine fibroids in the women uterus. However, the insufficiency of clinical interventions could result in tumor recurrence, and the defective tissues remained would cause intrauterine adhesions (IUAs) and further affect reproduction capacity. In this study, 3D printed hydrogel/poly(L-lactide-*co*-trimethylene carbonate) (PLLA-co-TMC, "PTMC" in short) core/shell scaffolds with NIR-tuned doxorubicin hydrochloride (DOX) and estradiol (E2) dual release were designed and fabricated for cancer therapy and uterine regeneration. Gelatin (Gel) and DOX were homogeneously mixed and then 3D printed to form Gel-DOX scaffolds. Gel-DOX scaffolds were then immersed in PTMC-PDA@E2 solution to fabricate Gel-DOX/PTMC-PDA@E2 core/shell scaffolds. Consequently, Gel-DOX/PTMC-PDA@E2 scaffolds could release DOX and E2 in a chronological manner, firstly delivering DOX assisted by phototherapy (PTT) to effectively kill Hela cells and then sustainably releasing E2 to promote uterine tissue regeneration. *In vitro* experiments showed that core/shell scaffolds exhibited excellent anticancer efficiency through the synergy of DOX release and hyperthermia ablation. Moreover, E2 could be sustainably released for over 28 days *in vitro* to promote the proliferation of bone marrow-derived mesenchymal stem cells (BMSCs). The novel Gel-DOX/PTMC-PDA@E2 core/shell scaffolds have therefore exhibited potential promise for the treatment of cancer therapy and uterine regeneration.

1 Introduction

According to the definition provided by the World Health Organization (WHO), infertility is the inability to achieve clinical pregnancy after 1-year regular unprotected intercourse. More than 14% of women at the reproductive ages suffered from infertility worldwide [1, 2]. Physical injuries, such as dilation and curettage and hysteroscopy adhesiolysis, or biochemical diseases, infections and tumors, or congenital uterine atrophy and malformation could cause the dysfunction of the uterus and thus result in infertility [3]. Among them, gynecologic cancers and uterine fibroids are the representative causes. According to American Cancer Society, 12-15% of cancers suffered by women are gynecologic cancers. Although most of gynecologic cancers occur in postmenopausal females, there are still about 20% in reproductive women yet. Particularly, 8% of endometrial, 12% of ovarian and 40% of cervical cancers occur in the childbearing age [4]. Moreover, uterine fibroids as the most common pelvic tumors and the most common benign tumors can happen in 60% of reproductive-aged women [5]. Uterine fibroids can potentially block the fallopian tubes or prevent the fertilized egg implanting in the uterus or inhibit a fetus from growing fully and cause miscarriage and thus result in infertility.

Many solutions, including surgical resection, radiation therapy, chemotherapy and hormone therapy, have been applied for gynecologic cancers and uterine fibroids treatment to restore fertility [6-10]. Surgical resection is one of the most used treatments for the cancerous tissues and uterine fibroids. However, the insufficiency of clinical interventions could result in tumor recurrence, and the defective tissues remained after surgical resection would cause intrauterine adhesions (IUAs) and further affect reproduction capacity. Therefore, a novel solution that can effectively kill residual tumor cells and at the same time regenerate the defective tissues should be developed . Inspired by the application of multifunctional scaffolds for tissue engineering and cancer treatment [11-14], 3D scaffolds having chemotherapy to eradicate tumor cells and regeneration capacity to reconstruct defective tissues after surgical resection could be a potential promise for cancer therapy and uterine regeneration. Especially, an on-demand dual drug/biomolecule delivery system responding to external stimuli would be more efficient for tumor cells elimination and stimulation of tissue regeneration [15-19].

Many studies have demonstrated that 3D scaffolds could release drugs or biomolecules on-demand triggered by various external stimuli, such as ultrasonic treatment, magnetic field, heat, near-infrared (NIR) laser irradiation, etc., to eradicate tumor cells and treat tissue defects [20-22]. Among those external stimuli, 3D scaffolds with NIR laser triggered drug or biomolecule release were one of the most used smart drug release systems for tumor cells eradication and tissue regeneration [12, 23-25]. 3D scaffolds incorporated with photothermal agents could induce photothermal effect and simultaneously stimulate drug or biomolecule release when irradiated by NIR laser. For example, polydopamine (PDA) particles are an excellent photothermal agent with good biocompatibility and biodegradability. Li *et al.* demonstrated that PDA particles could be heated up to ~60°C under 2.8 W/cm^2 808 nm NIR laser irradiation for 300s [26]. On one hand, the released anticancer drug and NIR-induced hyperthermia have a synergistic effect for tumor cells eradication. For example, our previous study has shown that bifunctional alginate/allylated gelatin hydrogels incorporated PDA particles (AlG/GelAGE-PDA@DOX hydrogels) exhibited anticancer synergy by providing combined chemotherapy and phototherapy for bone tumor cell ablation [14]. NIR laser irradiation could induce hyperthermia and meanwhile accelerate DOX release. On the other hand, NIR laser induced photothermal effect can increase the release of other drugs or biomolecules to promote tissue regeneration. Wan *et al.* indicated that PDA-coated hydroxyapatite nanoparticles (nHA@PDA) enabled to increase the release of osteogenic pargyline (PGL) to promote osteogenic differentiation of migrated cells and thus improve bone regeneration when irradiated by NIR laser. [27]. Previous studies have demonstrated promising efficacy in anticancer treatment or tissue regeneration through NIR laser-controlled drug release; however, the development of a dual drug/biomolecule release system that could release anticancer drugs first and subsequently sustainably release biomolecules for simultaneous cancer therapy and tissue regeneration remains less explored. Therefore, a dual drug/biomolecule release system tuned by NIR laser that could release anticancer drug and biomolecule (for tissue regeneration) in a chronological manner would be beneficial for gynecologic cancers and uterine fibroids treatment after surgical resection.

In the current study, to achieve chronological release of drug and biomolecule, 3D printed hydrogel/poly(L-lactide-*co*-trimethylene carbonate) (PLLA-co-TMC, "PTMC" in short) core/shell scaffolds with NIR laser-tuned DOX/estradiol (E2) release were

devised and fabricated for cancer therapy and uterine regeneration. DOX is a commonly used antineoplastic drug for many cancers treatment and has been clinically used for uterine cancers, and E2 is a biomolecule widely used to facilitate uterine regeneration [28-30]. 3D printed gelatin (Gel) scaffolds incorporated anticancer drug DOX (Gel-DOX scaffolds) were firstly fabricated. E2-containing PDA particles (PDA@E2 particles) were synthesized and characterized. Subsequently, Gel-DOX scaffolds were immersed in PTMC dichloromethane (DCM) solution incorporated PDA@E2 particles to engineer Gel-DOX/PTMC-PDA@E2 core/shell scaffolds (Fig.1A). PTMC coating layer improved the mechanical properties of the core/shell scaffolds and prolonged the degradation of Gel. In this study, Gel-DOX/PTMC-PDA@E2 core/shell scaffolds were designed to release DOX initially and quickly to effectively eradicate residual tumor cells after surgical resection and sustainably deliver E2 to promote uterine reconstruction (Fig.1B). Gel-DOX/PTMC-PDA@E2 core/shell scaffolds could controllably release DOX and E2 in a chronological manner. In detail, DOX could be rapidly released in 3 days to effectively kill the tumor cells assisted with NIR laser irradiation, and the release of E2 could last over 28 days to promote therapeutic effect for uterine regeneration. Therefore, Gel-DOX/PTMC-PDA@E2 core/shell scaffolds could exhibited potential promise for the treatment of cancer therapy and uterine regeneration.

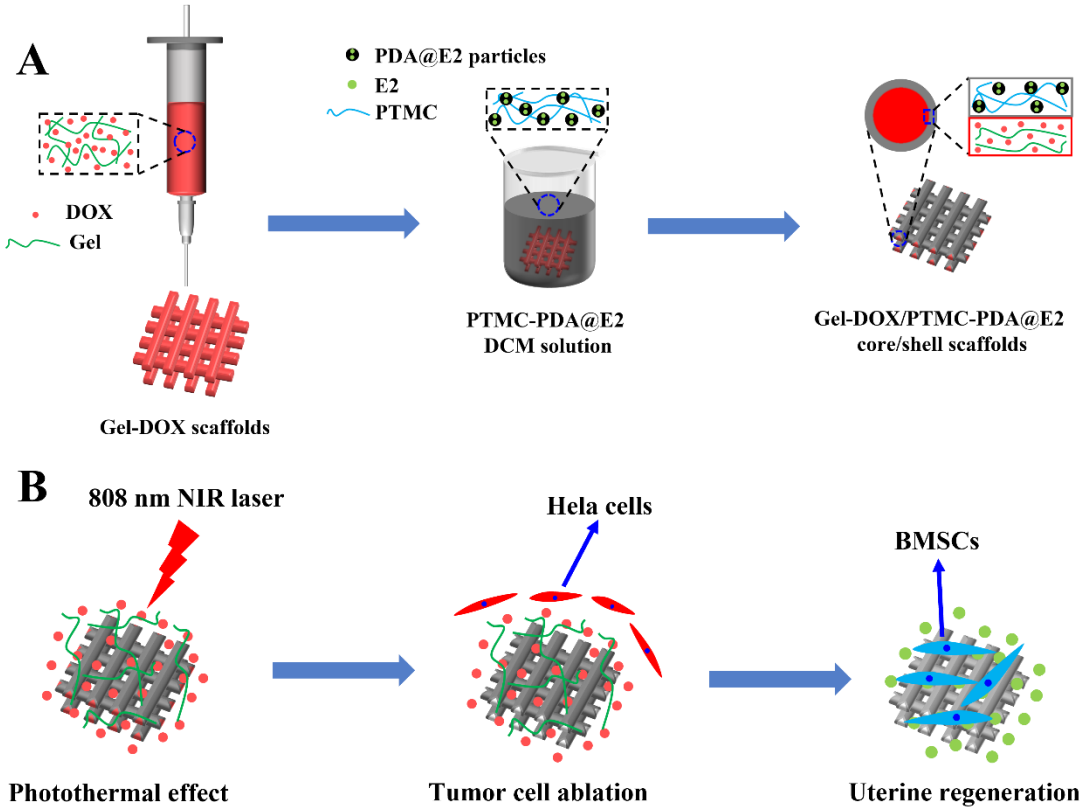

Fig.1 Schematic illustration of (A) Gel-DOX/PTMC-PDA@E2 core/shell scaffolds fabrication and (B) Gel-DOX/PTMC-PDA@E2 core/shell scaffolds releasing DOX and E2 in a chronological manner for cancer therapy and uterine regeneration.

2 Materials and methods

2.1 Materials

PTMC (molar ratio of LA: TMC = 5: 5, dl/g 0.9) was bought form Jinan Daigang Ltd., China. Dichloromethane (DCM) was bought from RCI Labscan Ltd., Thailand. Gelatin (porcine skin, type A, powder, gel strength ~300 g Bloom), dopamine hydrochloride, dimethyl sulfoxide, and 3-(4,5-dimethyl-2-thiazolyl)-2,5-diphenyl-2-H-tetrazolium bromide (MTT) assay were purchased from Sigma Aldrich (St. Louis, MO, USA). Estradiol (E2) and doxorubicin hydrochloride (DOX) were supplied by Aladdin Co. Ltd., China. Dulbecco's modified eagle medium (DMEM), fetal bovine serum (FBS), and penicillin-streptomycin (10,000 U/ml) were supplied by Gibco (Thermo Fisher Scientific, USA). The live/dead assay kits, Alexa Fluor™ 568 Phalloidin, and DAPI

were purchased from Invitrogen (Thermo Fisher Scientific, USA). Other reagents were provided by the local companies. All reagents were used as-received without further purification.

2.2 Synthesis of PDA and PDA@E2 particles

The synthesis process for PDA and PDA@E2 particles were similar with previous studies but with small modifications [31, 32]. Because E2 is poorly water-soluble, a water/ethanol (50/50 v/v) mixture was used to increase the solubility for PDA@E2 particles synthesis. 0.75g E2 was dissolved in 350ml ethanol under constant magnetic stirring for at least 2h. Subsequently, 12ml ammonia and 288ml DI water were added into ethanol solution under stirring for 30min. 2.5g dopamine hydrochloride was dissolved in 50ml DI water. Then, the dopamine solution was added into water/ethanol mixture under constant magnetic stirring for 24h at room temperature in the open air. Finally, PDA@E2 particles were centrifuged at 12,000 rpm for 10min and freeze-dried before storage. The morphology of PDA and PDA@E2 particles were characterized using a scanning electron microscope (SEM, Hitachi S-4800, Japan) and transmission electron microscope (TEM, Thermo Scientific Talos F200X, USA). The diameter distribution of PDA and PDA@E2 particles was measured using Image J software.

2.3 Fabrication of Gel-DOX/PTMC-PDA@E2 core/shell scaffolds

The Gel-DOX/PTMC-PDA@E2 core/shell scaffolds were fabricated according to the following process. 20 wt.% gelatin was dissolved in PBS at 50℃ water baths under magnetic stirring. DOX with a concentration at 2.0 mg/ml was then dissolved in Gel solution. After complete dissolution, the Gel-DOX solution was transferred to a printing cartridge on the 3D bioprinter (regenHU, Switzerland). The printing temperature was set at 30℃ and line distance was 2.0 mm. Nozzle inner diameter was 0.51 mm and the printing pressure was around 150-300 KPa. After 3D printing, scaffolds were freezing-dried.

Thereafter, different amount of PTMC was dissolved in DCM via ultrasonic and magnetic stirring to obtain PTMC solutions with different concentrations (5, 10, 20, and 25 wt.%). 2.5 wt.% PDA@E2 particles were homogeneously dispersed in PTMC solution to make PTMC-PDA@E2 solution via ultrasonic treatment and magnetic stirring. Afterwards, dried Gel-DOX scaffolds were soaked in PTMC-PDA@E2 DCM

solution for different time to prepare Gel-DOX/PTMC-PDA@E2 core/shell scaffolds. After coated for predetermined time, Gel-DOX/PTMC-PDA@E2 core/shell scaffolds were extracted from PTMC-PDA@E2 solution and placed in a fume hood to completely evaporate DCM. After evaporation, Gel-DOX/PTMC-PDA@E2 core/shell scaffolds were fabricated, with Gel-DOX serving as the core structure and PTMC-PDA@E2 forming the outer shell. Finally, the core/shell scaffolds were kept at 4℃ for further use.

2.4 Characterization of core/shell scaffolds

The macroscopic structure of Gel, Gel/PTMC and Gel/PTMC-PDA scaffolds was viewed by digital camera (Nikon). The overall morphology of Gel, Gel/PTMC and Gel/PTMC-PDA scaffolds was observed using an optical microscope (DMi8, Leica, Germany). Additionally, scaffolds were sputter-coated with a layer of gold nanoparticles, and then the microstructure of scaffolds was characterized via SEM. To visualize the cross-sectional microstructure, Gel, Gel/PTMC and Gel/PTMC-PDA scaffolds were broken in the liquid nitrogen and then observed via SEM. Moreover, Gel, Gel/PTMC and Gel/PTMC-PDA scaffolds were characterized via FT-IR analysis. The thermogravimetry analysis (TGA) was conducted to measure the relative weight percentages of PTMC and PTMC-PDA coating layer in Gel/PTMC and Gel/PTMC-PDA scaffolds, respectively.

2.5 Mechanical properties

The mechanical properties of Gel, Gel/PTMC, Gel/PTMC-PDA, and hollow PTMC scaffolds were analyzed via tensile tests by a universal material testing machine (Model 5848, Instron Ltd., USA) with a 100N load cell at room temperature. The tensile tests were conducted on at least 3 samples of each scaffold (30 × 10 × 1.5 mm). The upper and lower portions of each sample were clamped horizontally. The tension distance was 10 mm and the tension speed was 10 mm/min [33]. The tensile strength was determined as the highest stress and tensile strain was the break strain. The Young's modulus was determined by the slope of the initial linear range of stress-strain curves.

2.6 *In vitro* gelatin release and degradation

The gelatin release behavior of Gel, Gel/PTMC, and Gel/PTMC-PDA scaffolds was characterized by immersing samples in 5 ml PBS for 7 days. At each predetermined time interval, 1 ml PBS was extracted, and another 1 ml fresh PBS was added. The gelatin concentration of extracted medium was measured using BCA protein assay kit (Thermo Fisher Scientific, USA). The cumulative gelatin release curves were plotted.

To investigate *in vitro* degradation behavior of Gel, Gel/PTMC, Gel/PTMC-PDA, and hollow PTMC scaffolds, samples were soaked in PBS (supplemented with 0.02% sodium azide for antimicrobial) at 37 ℃ in an incubator with ~70 rpm/min shaking speed. The PBS was refreshed every two days. At each predetermined time interval, samples were collected and washed with DI water twice to remove the residual PBS. Afterward, samples were freezing-dried and weighted. The degradation rate of scaffolds was calculated by following formula:

$$\text{Degradation rate (\%)} = 100^* (M_0\text{-}M_s)/M_0 \qquad (1)$$

Where M_s represents the weight of dried samples at each predetermined time interval and M_0 represents the weight of initial dried samples [3].

2.7 Photothermal effect and *in vitro* drug release

The photothermal effect of Gel, Gel/PTMC, and Gel/PTMC-PDA scaffolds were evaluated by 808 nm NIR laser irradiation with different power densities (0.5 and 1.0 W/cm^2, respectively) for 3 min. The temperature of each sample was recorded using an infrared thermal camera (GUIDE® EasIR-9, AutoNavi, China) in real time.

To explore the *in vitro* DOX and E2 release behavior of Gel-DOX/PTMC-PDA@E2 core/shell scaffolds, samples were incubated in 5ml PBS in an incubator at 37 ℃ with ~70 rpm/min shaking speed. At predetermined time point, 1 ml PBS was extracted, and another fresh 1 ml PBS was added. The concentration of DOX was determined by UV-vis spectrometer (UV-2600, Shimadzu, Japan) at 480 nm, and the concentration of E2 of extracted medium was measured by UV-vis spectrometer at the wavelength of 280 nm.

On the other hand, to study the effect of 808 nm NIR laser irradiation on DOX and E2 release, Gel-DOX/PTMC-PDA@E2 samples were initially incubated in 5ml PBS at 37 ℃

for 30 min. Then, 1 ml PBS was extracted, and another 1 ml fresh PBS was added. Afterward, samples were irradiated by 808 nm NIR laser (0.5 and 1.0 W/cm^2, respectively) for 30 min, and 1 ml PBS was collected, and another 1 ml fresh PBS was added. This cycle will last 3 times. The concentration of DOX and E2 was determined by UV-vis spectrometer at 480 nm and 280 nm, respectively.

2.8 *In vitro* antitumor efficiency

The Hela cells (Sigma Aldrich, USA) were employed to investigate the antitumor efficiency of Gel-DOX/PTMC-PDA@E2 scaffolds. Hela cells were seeded in 24-well cell culture plate at a density of 1×10^4 cells per well and cultured in DMEM supplemented 10% fetal bovine serum and 1% penicillin/streptomycin at 37 ℃ for 48 h. Subsequently, cells were treated as the following five groups: 1) without any treatment (control); 2) treatment with Gel/PTMC-PDA scaffolds (Gel/PTMC-PDA); 3) treatment with Gel/PTMC-PDA scaffolds plus 808 nm NIR laser irradiation for 5 min per day (Gel/PTMC-PDA + NIR); 4) treatment with Gel-DOX/PTMC-PDA scaffolds (Gel-DOX/PTMC-PDA) and (5) treatment with Gel-DOX/PTMC-PDA scaffolds plus 808 nm NIR laser irradiation for 5 min per day (Gel-DOX/PTMC-PDA + NIR). After cultured for 4, 24, and 72 h, the live/dead assay (Thermo Fisher Scientific, USA) and MTT assay were used to visually observe the viability of Hela cells. In detail, Hela cells were stained by working solution (4 μM EthD-1, 2 μM AM dissolved in PBS) for 20 min at room temperature. Living cells were stained green and dead cells were stained red when observed under fluorescence microscope (DMi8, Leica, Germany). The cell survival rate was calculated using Image J software.

2.9 *In vitro* biological evaluation

To evaluate the biological properties of core/shell scaffolds, dried scaffolds were sterilized via gamma irradiation for 20 min and then cultured in low glucose DMEM supplement with 10% FBS and 1% penicillin/streptomycin at 37 ℃ incubator. BMSCs (human, Lonza, Switzerland) at passage 5-8 were used.

To explore the cell survival, BMSCs at the density of 2×10^4 cells per well were seeded on Gel/PTMC, Gel/PTMC-PDA, and Gel/PTMC-PDA@E2 scaffolds in 24 well cell culture plate, respectively. After cultured for 4, 24, and 48 h, samples were washed with PBS and then stained with working solution (4 μM EthD-1, 2 μM AM dissolved in PBS)

for 20 min at room temperature. The cell morphology on scaffold samples were observed using fluorescence microscope (DMi8, Leica, Germany). The cell survival rate was calculated using Image J software. For cell proliferation, BMSCs at the density of 1×10^4 cells per well were seeded on the samples. After cultured for 1, 3, and 7 days, BMSCs proliferation behavior was examined using MTT tests. Briefly, 5 mg/ml MTT solution was mixed with DMEM at the ratio of 1:9 to prepare working solution. At each culture time point, prepared working solution was added and incubated at 37 ℃ for 4 h. After reaction, the solution was discarded and DMSO was added to dissolve formazan. The OD value of each sample was measured using microplate reader at 540 nm. Additionally, BMSCs morphology was visualized by F-actin and DAPI staining. After cultured for 1, 3, and 7 days, samples were immobilized with 4.0% paraformaldehyde (PFA) for 20 min in dark. After washing with PBS twice, samples were treated with 0.1% Trixton-100 for 20 min and blocked with 1% bovine serum albumin for 1 h. Subsequently, samples were stained with Alexa Fluor 568 phalloidin (Invitrogen, Thermo Fisher Scientific) and DAPI (Invitrogen, Thermo Fisher Scientific) solutions. The BMSCs morphology was visualized using confocal laser scanning microscope (CLSM, Leica, Germany).

2.10 Statistically analysis

The results presented in this article were obtained from at least 3 separate experiments and are expressed as the mean ± SD. The one-way ANOVA was performed for statistical analysis. Statistically significant difference existed when: $*p < 0.05$, $**p < 0.01$, and $***p < 0.001$.

3 Results and Discussion

3.1 Synthesis and characterization of PDA and PDA@E2 particles

E2 is an efficient biomolecule for uterine regeneration [34]. E2 could bind to the estrogen receptors and thus activate a cascade of biochemical reactions and further promote endometrial epithelium cells proliferation and endometrium regeneration [35]. However, the poor water solubility and limited half-life time may lead to the low efficiency of estrogen therapy. Oral administration usually results in low concentration of E2 in the injured sites. The encapsulation of E2 in drug carriers or vehicles could overcome these limitations. For example, Zhang *et al.* injected the Heparin-Poloxamer

(HP) hydrogels loaded with E2 into the injured uterine cavity in SD rats. They found that sustainable release of E2 could significantly facilitate the regeneration of injured endometrium and upregulation of kisspeptin via the activation of ERK1/2 and MAPKs p38 pathways [28].

Many nanoparticles have been designed as efficient drug carriers or vehicles to release the cargo sustainably and controllably in site, thus achieving long-term therapeutic effect [36-38]. Among these nanoparticles, PDA particles have been defined as a versatile and promising drug carrier for tissue regeneration because of good biocompatibility and biodegradability and excellent photothermal effect [14, 39, 40]. Additionally, due to the inherent catechol and anthracene moieties on the PDA surface, many drugs and biomolecules could be efficiently encapsulated in PDA particles via Michael addition reaction or Schiff base reaction under alkaline condition [41]. Moreover, many studies reported that PDA particles could release drugs or biomolecules sustainably and controllably and thus promote tissue regeneration [42].

In the current study, inspired by their intrinsic advantages, PDA nanoparticles were used to encapsulate E2. To increase the E2 solubility, a 50/50 v/v ethanol/water mixture was employed for PDA@E2 particles synthesis. As shown in Fig.2, the SEM and TEM images showed that PDA and PDA@E2 nanoparticles exhibited similar microstructure. Both PDA and PDA@E2 nanoparticles were spherical in shape. Fig.2A3&B3 show the particle size distribution of PDA and PDA@E2 nanoparticles. The diameter of PDA and PDA@E2 nanoparticles was 190.5 ± 4.9 nm and 182.7 ± 16.6 nm, respectively (Fig.S1A). Notably, the incorporation of E2 in PDA particles showed little effect on microstructure and diameter of particles. Moreover, the FT-IR spectra in Fig.S1B displayed the characteristic functional groups of E2, PDA and PDA@E2. The peaks at 3437 cm^{-1} and 3205 cm^{-1} in the spectrum of E2 could be attributed to the -OH at C-3 and C-17 positions, respectively. The peaks at 1609 cm^{-1} and 1498 cm^{-1} could be assigned as aromatic double bonds [43]. Peaks in the range of 2980 – 2800 cm^{-1} were related to the C-H vibration [44]. Additionally, the broad band from 3600-3000 cm^{-1} in the spectrum of PDA was due to N-H and O-H stretching. The peaks at 1575 cm^{-1} and 1504 cm^{-1} could be responding to the C=C band of indole, and the peak at 1162 cm^{-1} might be attributed to the C-N stretching in indolequinone [45]. The spectrum of

PDA@E2 displayed the characteristic C-N stretching at 1157 cm^{-1} and C-H vibration in the range of 2980 – 2800 cm^{-1}, suggesting the encapsulation of E2 in PDA particles.

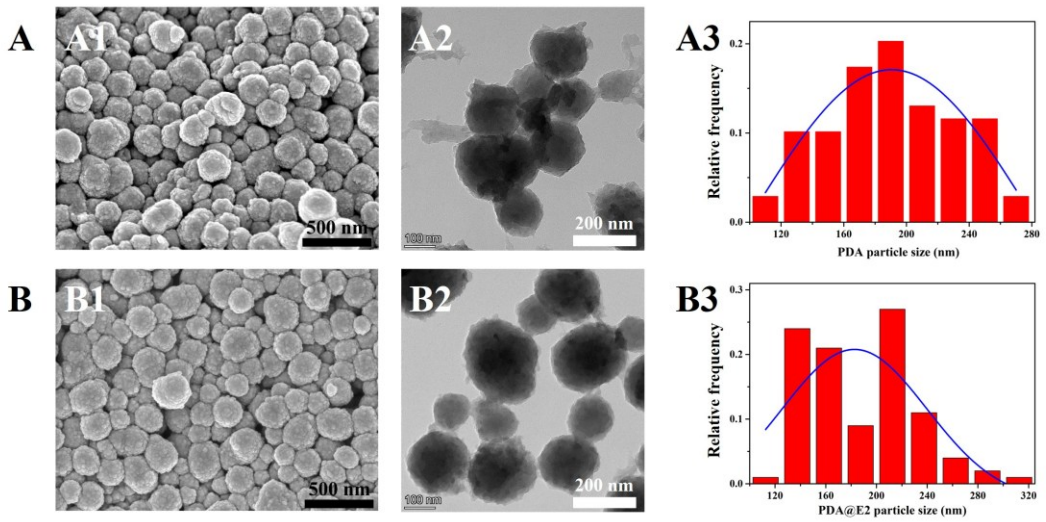

Fig.2 Characterization of PDA and PDA@E2 particles. (A1, B1) SEM images and (A2, B2) TEM images showing the microstructure of (A) PDA and (B) PDA@E2 particles. (A3, B3) Particle size distribution of PDA and PDA@E2 particles.

3.2 Fabrication and characterization of Gel-DOX/PTMC-PDA@E2 core/shell scaffolds

Due to excellent biocompatibility and biodegradability and thermosensitive properties, gelatin is a potential natural polymer that have been widely used in tissue regeneration and drug release [46-48]. But the problem is that Gel could be quickly degraded in the physiological environment if without crosslinking and the degradation duration could be several hours [49, 50]. In the current study, DOX was mixed with Gel to prepare Gel-DOX scaffolds via 3D printing. To avoid burst release and prolong the DOX release duration, Gel-DOX scaffolds were coated with PTMC polymer on the surface by dip coating. PTMC could cover the entire surface of 3D printed Gel-DOX filaments and thus effectively delay the Gel degradation and prevent the quick leakage of the loaded DOX from scaffolds. As shown in Fig.3A&B, the thickness of PTMC could precisely controlled by the concentrations of PTMC solutions and soaking time. PTMC solution with high concentration exhibited high viscosity, which would make more PTMC coated on the scaffold surface and thus increase the PTMC layer thickness

(Fig.S2). The higher concentration of PTMC solution, the greater of its viscosity, making a higher thickness of PTMC shell. Notably, there was no difference about PTMC layer thickness when soaking Gel scaffolds in 25% PTMC solution over 10 min (Fig.3B). Therefore, immersing Gel scaffolds in 25% PTMC solution for 10 min was used to fabricate core/shell scaffolds for further experiments.

TGA results in Fig.S3A indicated that Gel and PTMC started to decompose at 85 ℃ and 264 ℃, respectively. When PTMC was nearly thermally decomposed at 428 ℃, the residual mass percentages of Gel, Gel/PTMC, and Gel/PTMC-PDA scaffolds were 38.52%, 20.48%, and 19.71%, respectively. Furthermore, as shown in Fig.S3B, Gel scaffolds exhibited characteristic Amide I, II, and III peaks at 1634 cm^{-1}, 1538 cm^{-1}, and 1236 cm^{-1} [51]. After deposited PTMC and PTMC-PDA layer on the Gel scaffolds surface, only the characteristic C=O peak at 1739 cm^{-1} and C-O-C peaks in the range of 1100-1300 cm^{-1} of PTMC appeared [52], suggesting PTMC and PTMC-PDA entirely covered Gel scaffolds surface.

Fig.S4 shows the macroscopic photo of Gel, Gel/PTMC, and Gel/PTMC-PDA scaffolds. After coated with PTMC-PDA layer, the appearance of the scaffold turned into black from white. The optical microphages and SEM images in Fig.3C&D displayed the surface morphology and microstructure of Gel, Gel/PTMC, and Gel/PTMC-PDA scaffolds. It can be clearly seen the presence of PDA particles in the Gel/PTMC-PDA scaffold in Fig.3C. In addition, many small pores appeared on the Gel/PTMC, and Gel/PTMC-PDA scaffolds surface, which might result from the evaporation of DCM (Fig.3D). After coating, the diameter of Gel/PTMC, and Gel/PTMC-PDA scaffolds obviously increased. The cross-sectional view in Fig.4 indicated that PTMC and PTMC-PDA layers were closely attached to the Gel scaffolds surface, and the thickness of PTMC and PTMC-PDA layers was about 100 μm. As a result, the PTMC and PTMC-PDA coating layer could prevent rapid degradation of Gel and thus prolong the release duration of encapsulated DOX. Moreover, since PDA@E2 particles were loaded in the PTMC layer, the PTMC-PDA@E2 coating layer was supposed to release E2 controllably and sustainably to promote uterine regeneration.

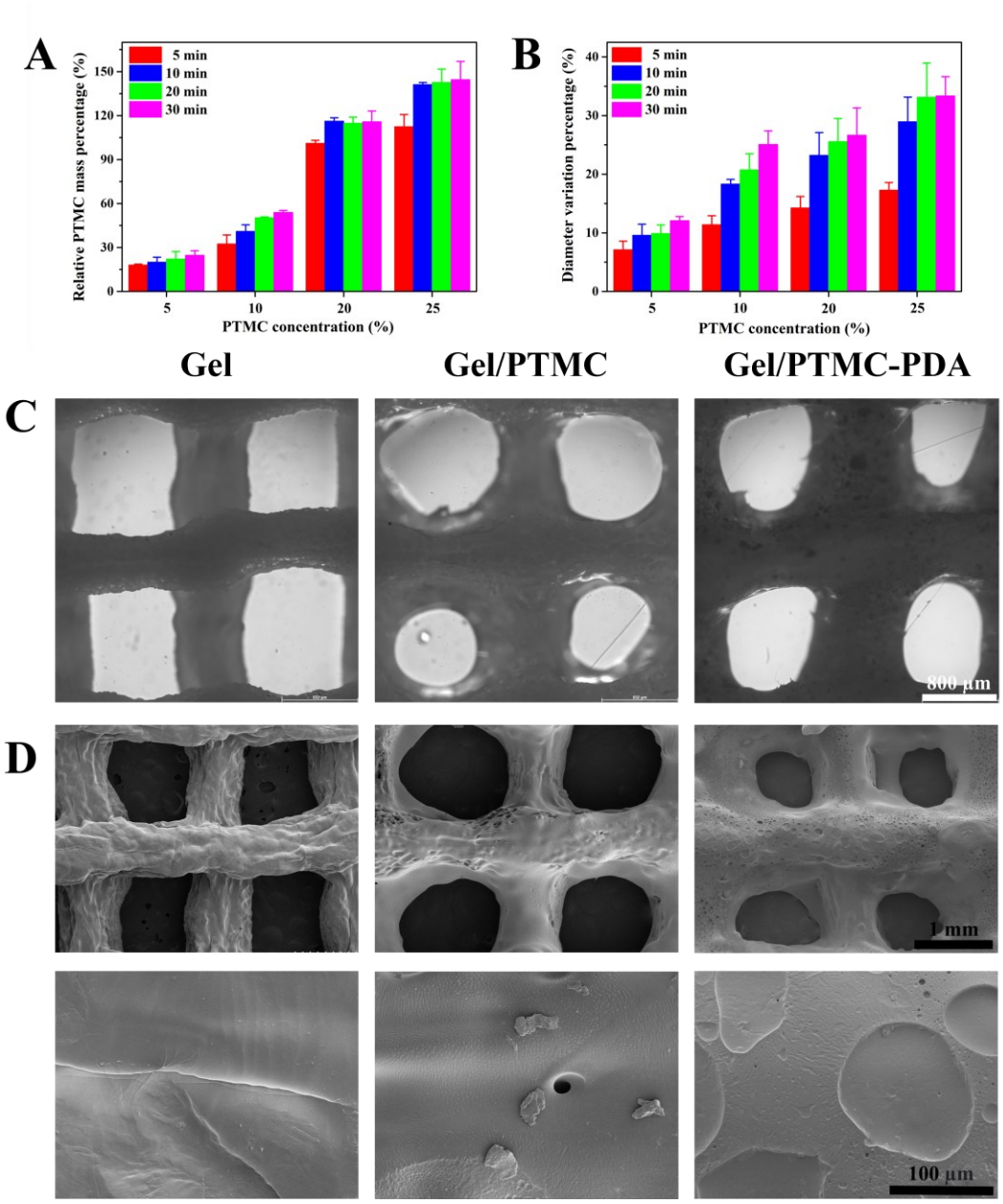

Fig.3 Characterization of the core/shell scaffolds. (A) The relative PTMC mass percentage and (B) diameter variation percentage of Gel/PTMC scaffolds after immersing Gel scaffolds in different concentrations of PTMC solutions for different time. (C) Optical micrographs and (D) SEM images showing the morphology and structure of Gel, Gel/PTMC, and Gel/PTMC-PDA scaffolds.

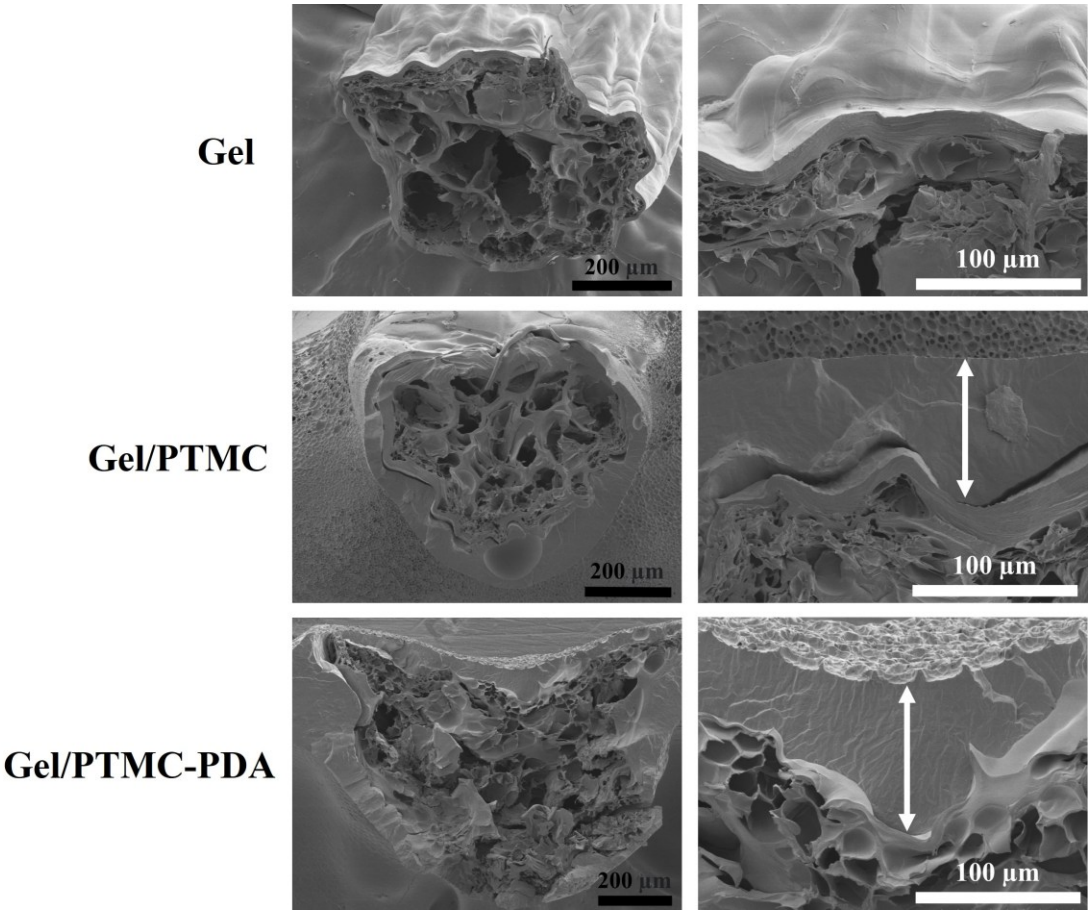

Fig.4 SEM images showing the cross-sectional morphology of Gel, Gel/PTMC, and Gel/PTMC-PDA scaffolds. The white double arrow lines represent PTMC and PTMC-PDA shell.

3.3 Mechanical properties

The mechanical properties of tissue engineering scaffolds should be comparable to the target tissues. In the current study, Gel/PTMC-PDA core/shell scaffolds were supposed to have comparable mechanical performance to the native uterine tissues. Previous *ex vivo* studies revealed that the ultimate tensile strength of porcine uterine tissue was 320 ± 176 KPa with a corresponding strain at 30 ± 9.0%, while the average ultimate tensile strength of the women uterus was 656.3 ± 483.9 KPa at the strain of 32 ± 11.2% [53, 54]. Another study indicated that the mechanical strength of uterine tissues was 258 ± 71 KPa [55]. Moreover, the *in vivo* tension test indicated that the tensile strain of the women uterus could be in the range of 110-130% [56, 57]. The mechanical properties of core/shell scaffolds were assessed via tensile tests in both dry and wet states. Notably, the PTMC and PTMC-PDA coating layer significantly promoted the mechanical

strength of scaffolds. As shown in Fig.5, the tensile strength of Gel, Gel/PTMC, Gel/PTMC-PDA, and hollow PTMC scaffolds in wet state was 4.20 ± 0.52 KPa, 70.60 ± 4.68 KPa, 117.36 ± 10.68 KPa, and 73.83 ± 10.20 KPa, respectively. Additionally, scaffolds exhibited higher tensile strain after coated with PTMC and PTMC-PDA layer. The strain of Gel, Gel/PTMC, Gel/PTMC-PDA, and hollow PTMC scaffolds was 37.02 ± 4.63%, 247.03 ± 26.71%, 182.01 ± 20.61%, and 187.60 ± 24.52%. Consequently, the Young's modulus of Gel, Gel/PTMC, Gel/PTMC-PDA, and hollow PTMC scaffolds was 14.38 ± 2.12 KPa, 90.53 ± 15.11 KPa, 217.53 ± 4.43 KPa and 104.87 ± 13.83 KPa, respectively. On the other hand, the mechanical strength of dried Gel, Gel/PTMC, and Gel/PTMC-PDA scaffolds was 1.23 ± 0.07 MPa, 4.11 ± 0.34 MPa, and 4.48 ± 0.45 MPa, respectively (Fig.S5). Compared with wet state, dried core/shell scaffolds possessed much higher tensile strength, but the tensile strain dramatically decreased. The tensile strain of Gel, Gel/PTMC, and Gel/PTMC-PDA scaffolds was 6.78 ± 0.21%, 27.32 ± 7.61%, and 21.54 ± 0.79%. Notably, core/shell Gel/PTMC-PDA scaffold whether in wet or dry state possessed comparable mechanical performance to the native uterine tissues, suggesting that Gel/PTMC-PDA scaffold could be a potential promise for uterine regeneration.

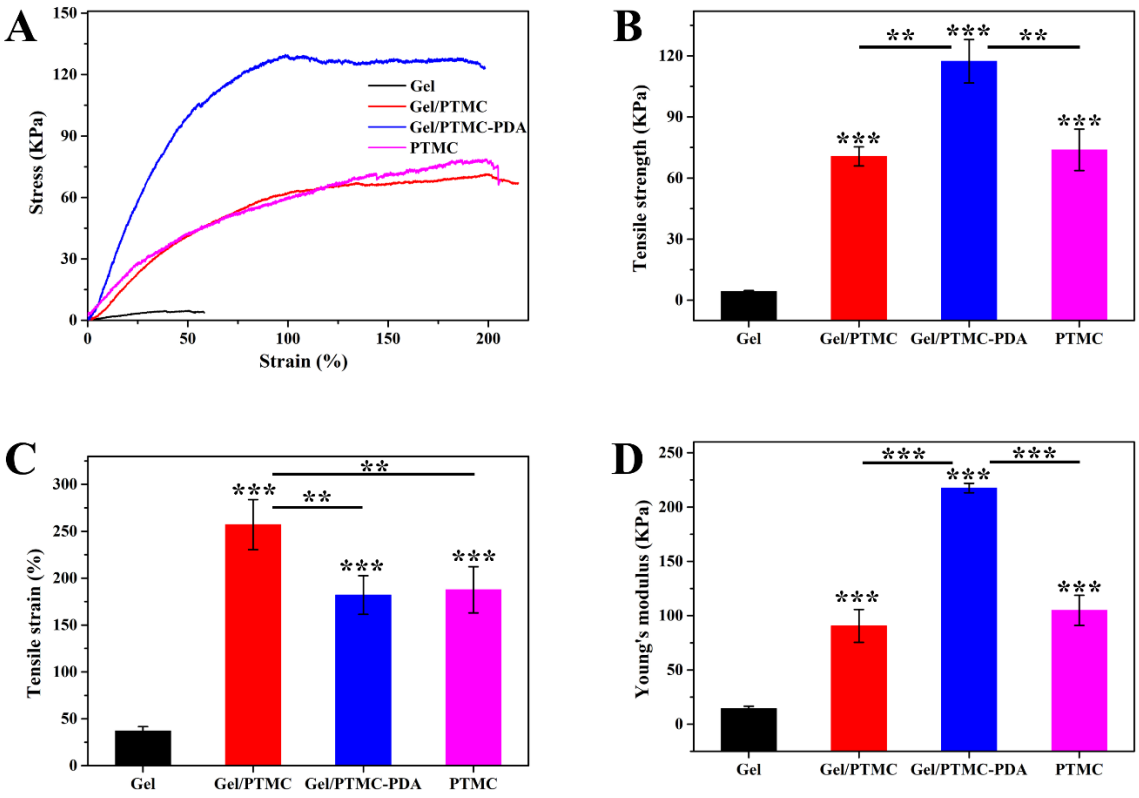

Fig.5 The mechanical properties of Gel, Gel/PTMC, Gel/PTMC-PDA and hollow PTMC scaffolds in wet state. (A) Stress-strain curves, (B) tensile strength, (C) tensile strain and (D) Young's modulus of Gel, Gel/PTMC, Gel/PTMC-PDA and hollow PTMC scaffolds.

8.3.4 *In vitro* gelatin release and degradation

The degradation behavior of the core/shell scaffolds was studied *in vitro* by culturing scaffolds in PBS (0.01M, pH 7.4) at 37 ℃. In this study, PTMC shell was constructed to protect gelatin from rapid degradation and thus inhibit rapid DOX release. The gelatin release kinetic was firstly investigated. As shown in Fig.6A, gelatin was quickly released from Gel scaffolds in several hours. In contrast, the gelatin release was much slower in Gel/PTMC and Gel/PTMC-PDA scaffolds. The release of gelatin could last more than 3 days. The TGA results in Fig.6B also showed that when PTMC was nearly entirely thermally degraded, the residual mass percentages of Gel/PTMC and Gel/PTMC-PDA scaffolds after 1d degradation were 17.0% and 16.5%, respectively. After 3 days degradation, owing to the continuous gelatin release, the mass percentages of Gel/PTMC and Gel/PTMC-PDA scaffolds decreased to 11.0% and 8.0%. When gelatin was completely released at 7 days culture, the residual mass percentages of Gel/PTMC and Gel/PTMC-PDA scaffolds were 0.2% and 4.5%. Moreover, Fig.6C further showed the surface and cross-sectional morphology of scaffolds after degradation. It could be clearly seen the presence of gelatin in the core of scaffolds after 1- and 3-day degradation. It is well-known that gelatin without crosslink can be rapidly degraded in several hours [58, 59]. In the current study, PTMC and PTMC-PDA layer were coated on the scaffolds surface to prevent gelatin from quick release. As a result, the coating layer could prolong the release of gelatin to more than 3 days, suggesting that core/shell scaffolds could inhibit the rapid release of DOX and extend the DOX release duration over 3 days and thus promote the antitumor efficiency.

Fig.6D indicated that Gel had a very quick degradation rate and PTMC had a slow degradation rate. After 12 weeks culture, only ~10% weight of PTMC was degraded. On the other hand, the degradation behavior of Gel/PTMC and Gel/PTMC-PDA scaffolds were nearly the same. About 60 wt.% of Gel/PTMC and Gel/PTMC-PDA scaffolds remained after 3 days incubation. The possible reason might be that the core gelatin, which is about 40 wt.% of the core/shell scaffolds (Fig.3A), was quickly

degraded. Afterward, the degradation rate of the scaffolds became much slower. After 12 weeks incubation, the degradation rates of Gel/PTMC and Gel/PTMC-PDA scaffolds were 59.11 ± 3.54% and 56.25 ± 4.41%, respectively.

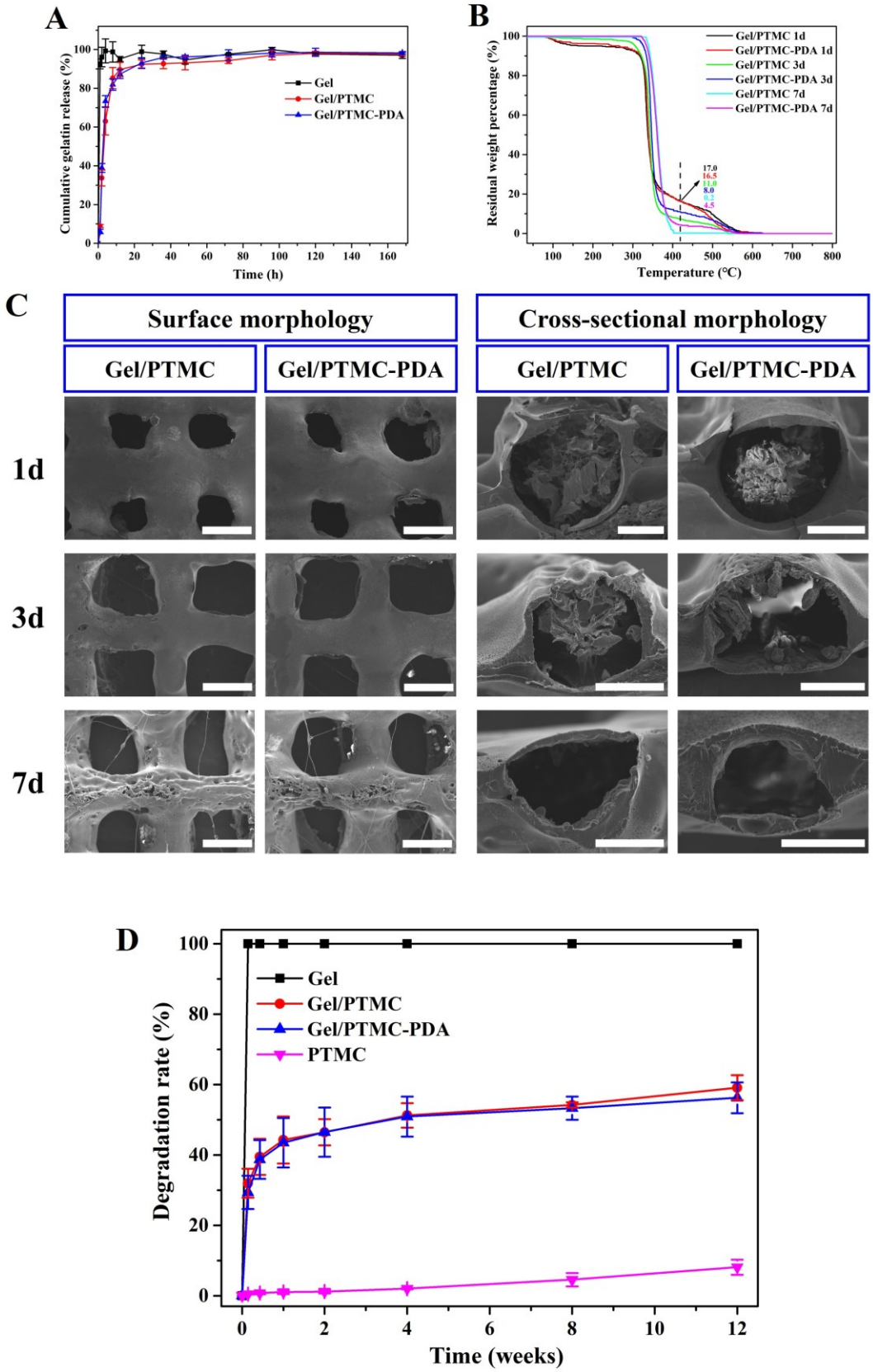

Fig.6 *In vitro* gelatin release. (A) The cumulative gelatin release percentage from Gel, Gel/PTMC, and Gel/PTMC-PDA scaffolds in 7 days. (B) The TGA

results of Gel/PTMC and Gel/PTMC-PDA scaffolds after being immersed in PBS for 1, 3, and 7 days. (C) SEM images showing the surface and cross-sectional morphology of Gel/PTMC and Gel/PTMC-PDA scaffolds after being immersing in PBS for 1, 3, and 7 days. The scale bar: 1 mm for surface and 500 μm for cross-sectional view. (D) The degradation behavior of Gel, Gel/PTMC, Gel/PTMC-PDA, and hollow PTMC scaffolds.

3.5 Photothermal effect and *in vitro* drug release

PDA particles are excellent photothermal agent and drug vehicle [40, 41]. PDA@E2 particles exhibited high loading efficiency and excellent photothermal conversion capability. Incorporating PDA@E2 particles in PTMC shell made good photothermal effect and controlled E2 release of core/shell scaffolds. The photothermal conversion efficiency of scaffolds was investigated by exposing scaffolds under NIR laser irradiation (0.5 W/cm^2 and 1.0 W/cm^2). As shown in Fig.7A-C, the temperatures of Gel and Gel/PTMC scaffolds did not change too much after irradiated by NIR laser for 3 min. In contrast, Gel/PTMC-PDA scaffolds could be heated up to 48 ℃ and 56.7 ℃ when irradiated by 808nm NIR laser at density of 0.5 W/cm^2 and 1.0 W/cm^2 for 3min, respectively, suggesting high photothermal conversion capacity of Gel/PTMC-PDA scaffolds. Previous study indicated that when the local temperature raised up to over 42 ℃ under NIR laser irradiation, the residual tumor cells could be effectively killed [60]. Therefore, core/shell scaffolds could facilitate hyperthermia ablation of tumor cells after the implantation at the original tumor site of the body.

On the other hand, the good photothermal effect made Gel/PTMC-PDA scaffolds possessing the capacity of NIR laser-triggered on demand drug release. Due to the high photothermal conversion capacity, core/shell scaffolds could be quickly heated and thus accelerate drug release, realizing desired therapeutic effect. Fig.7D shows the DOX release profiles of Gel-DOX, Gel-DOX/PTMC, and Gel-DOX/PTMC-PDA scaffolds. The DOX release was mainly tuned by gelatin degradation and the DOX release rate was similar with gelatin degradation rate (Fig.6A). As shown in Fig.7D, compared to that DOX was entirely released from Gel-DOX scaffold in several hours, Gel-DOX/PTMC and Gel-DOX/PTMC-PDA scaffolds could sustainably release DOX for

more than 3 days. Furthermore, the DOX release behavior of Gel-DOX/PTMC-PDA scaffolds triggered by NIR laser irradiation is shown in Fig.7E. After being irradiated by NIR laser, the DOX release rate was increased. With the density of NIR laser increased, more DOX released. NIR laser exposure could increase the local temperature. High temperature facilitated Brownian movement and accelerated the gelatin degradation and thus promoted DOX release. As a result, Gel-DOX/PTMC-PDA scaffold could controllably release DOX on demand by tuning the irradiation of NIR laser.

Since the mammalian uterus has a dynamic pH microenvironment, it is essential to investigate E2 release behavior of the core/shell scaffolds in different pH buffers. Therefore, to mimic the microenvironment of uterine tissues, three different pH buffers (pH 4.5, 7.4, and 9.0) were employed to investigate the *in vitro* E2 release kinetics in this study. As shown in Fig.7F, the E2 release was pH-sensitive, and the release kinetics in different pH solutions could match the Higuchi model (Fig.S6). E2 could be quickly released in the basic solution (pH 9.0) while slowly released in the acidic solution (pH 4.5). This could result from the pH-responsive behavior of PDA particles [61, 62] and PTMC degradation [63]. PDA particles are a pH-responsive biomaterial, exhibiting different solubility and degradation behavior at varying pH environments. Generally, at acidic pH environment, the catechol and amine groups in PDA are protonated, leading to increased swelling and degradation of the PDA particles, resulting in a faster release of the encapsulated drugs. In contrast, under neutral or basic condition, the PDA particles remain more stable, resulting in a slower release of the drugs. However, in the current study, E2 was quickly released in the basic solution. It could mainly be attributed to the degradation of PTMC polymer. Since PDA@E2 particles were encapsulated within the PTMC shell, which exhibits lower hydrophilicity, their behavior remains unaffected by external factors until they are released from the PTMC shell. Considering the rapid degradation of PTMC in alkaline conditions, it is unsurprising that the release of E2 exhibits a slower rate in an acidic environment. In this study, DOX was designed to be rapidly released in 3 days to effectively kill the residual tumor cells while E2 was expected to be sustainably released to promote uterine regeneration in a long-term period. As depicted in Fig.7F, E2 could be sustainably released for over 28 days in different pH solutions. It is well-known that long-term biomolecule release enables to extend the therapeutic effect and thus promote

tissue regeneration [64, 65]. The sustained E2 release could continuously bind to its receptors and then stimulate the expression of angiogenic growth factors, such as vascular endothelial growth factor (VEGF), fibroblast growth factors (FGFs), and transforming growth factors (TGFs) [66]. Those angiogenic growth factors would increase blood vessel density and improve the uterine reconstruction. On the other hand, similar to the DOX release, E2 release behavior could also be tuned by NIR laser irradiation (Fig.7G). When exposed to 808 nm NIR laser irradiation, the E2 release increased. Additionally, with more density of NIR laser, more E2 was released. Given the excellent photothermal conversion efficiency of PDA particles, exposure to NIR laser irradiation could cause a localized temperature rise in the PDA particles. The increase in temperature resulting from NIR irradiation induced structural changes in the PDA matrix, loosening the interaction between the PDA and E2 and consequently expediting the release of E2 as the intermolecular bonds between the PDA matrix and E2 progressively weaken. Additionally, high temperature facilitated Brownian movement (molecular motion). The increase in molecular motion helped E2 to diffuse out of the PDA particles more quickly and thus promoted E2 release.

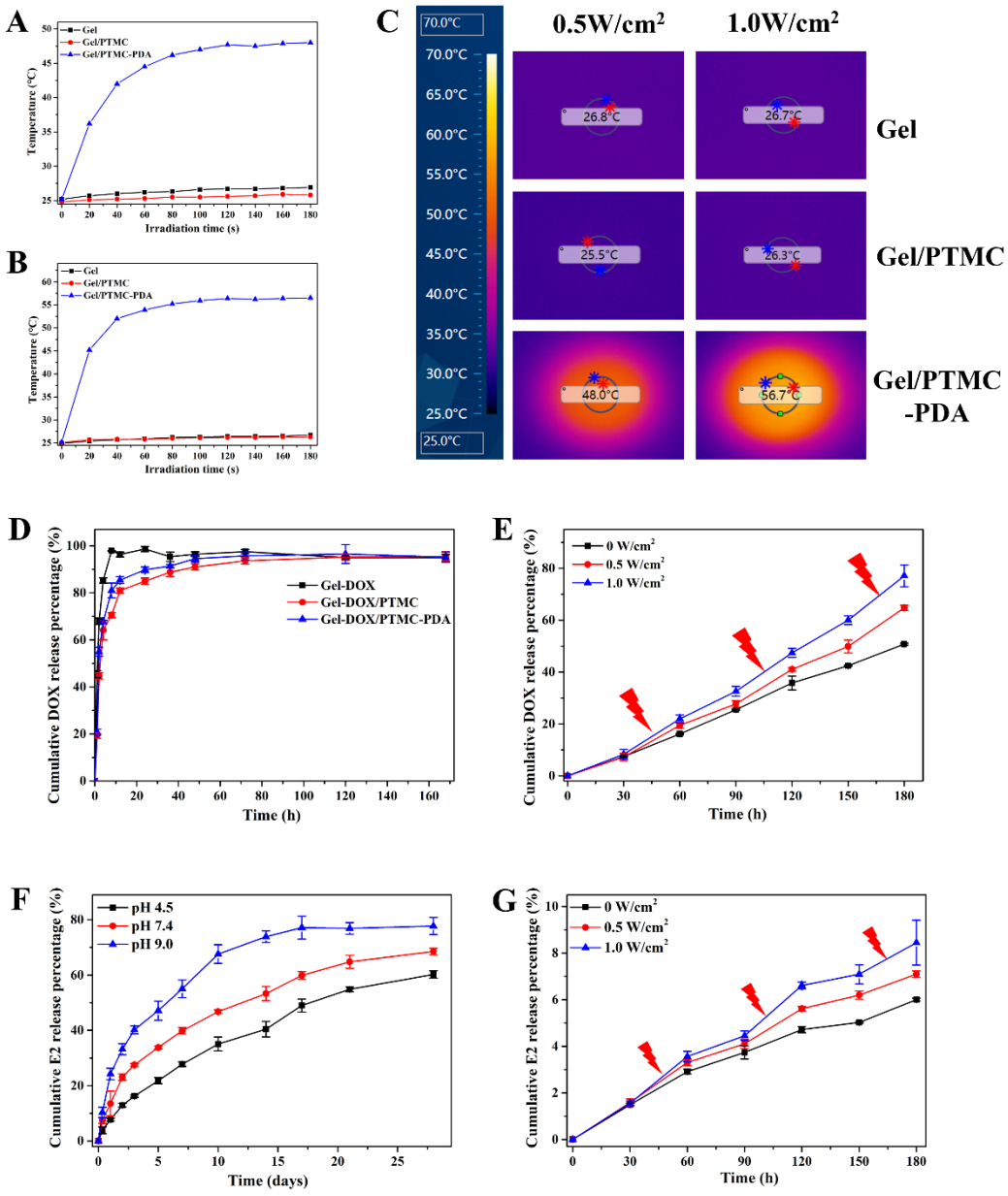

Fig.7 Photothermal effect and *in vitro* drug release of core/shell scaffolds. The temperature variation of Gel, Gel/PTMC, and Gel/PTMC-PDA scaffolds after being irradiated by NIR laser with density of (A) 0.5 W/cm^2 and (B) 1.0 W/cm^2. (C) The infrared thermal images of Gel, Gel/PTMC, and Gel/PTMC-PDA scaffolds after being irradiated by NIR laser with density of 0.5 W/cm^2 and 1.0 W/cm^2 for 3min. (D) *In vitro* DOX release kinetics of Gel-DOX, Gel-DOX/PTMC and Gel-DOX/PTMC-PDA scaffolds. (E) *In vitro* cumulative DOX release profiles of Gel-DOX/PTMC-PDA scaffolds with (0.5 W/cm^2 and 1.0 W/cm^2) and without NIR laser irradiation. (F) *In vitro* cumulative E2 release profiles of Gel/PTMC-PDA@E2 scaffolds in pH 4.5, 7.4, and 9.0

buffer solutions. (G) *In vitro* cumulative E2 release behavior of Gel /PTMC-PDA@E2 scaffolds with (0.5 W/cm^2 and1.0 W/cm^2) and without NIR laser irradiation.

3.6 *In vitro* antitumor efficiency of the core/shell scaffolds

Chemotherapy assisted by PTT can controllably release DOX on site and simultaneously provide hyperthermia, showing great synergy for tumor treatment [67, 68]. Many studies have reported that NIR laser irradiation could stimulate DOX release and synergistically induce high temperature for improved anticancer therapy [69, 70]. In the current study, the antitumor efficiency of core/shell scaffolds was evaluated. As shown in Fig.8A, many dead cells appeared in Gel/PTMC-PDA+NIR laser, Gel-DOX/PTMC-PDA and Gel-DOX/PTMC-PDA+NIR laser groups. Moreover, Fig.8B showed that the cell survival rates of Gel/PTMC-PDA+NIR laser, Gel-DOX/PTMC-PDA, and Gel-DOX/PTMC-PDA+NIR laser groups, after cultured for 72h, were 70.31 ± 2.35%, 24.07 ± 8.71%, and 8.29 ± 3.55%, respectively. Compared to Gel/PTMC-PDA group, the cell survival rate of Gel/PTMC-PDA+NIR laser group significantly decreased, which could be attributed to the hyperthermia triggered by NIR laser irradiation. Previous study has demonstrated that high temperature (usually over 42 ℃) resulted from photothermal effect under the NIR laser irradiation exhibited positive effect on tumor cells ablation [60, 71]. DOX could be continuously released in 3 days and cell survival rate was increasingly dropped with the culture time. Moreover, with synergy of NIR laser irradiation, induced hyperthermia could accelerate gelatin degradation and DOX release, leading to greatly kill the tumor cells and dramatically decrease the cell survival rate. The dramatically decreased cell viability of Gel-DOX/PTMC-PDA+NIR laser group in Fig.8C further confirmed the synergy of chemotherapy and PTT for tumor cell eradication. As a result, Gel-DOX/PTMC-PDA scaffolds with NIR laser irradiation performed excellent antitumor efficiency and could significantly kill the tumor cells with synergy of chemotherapy and PTT.

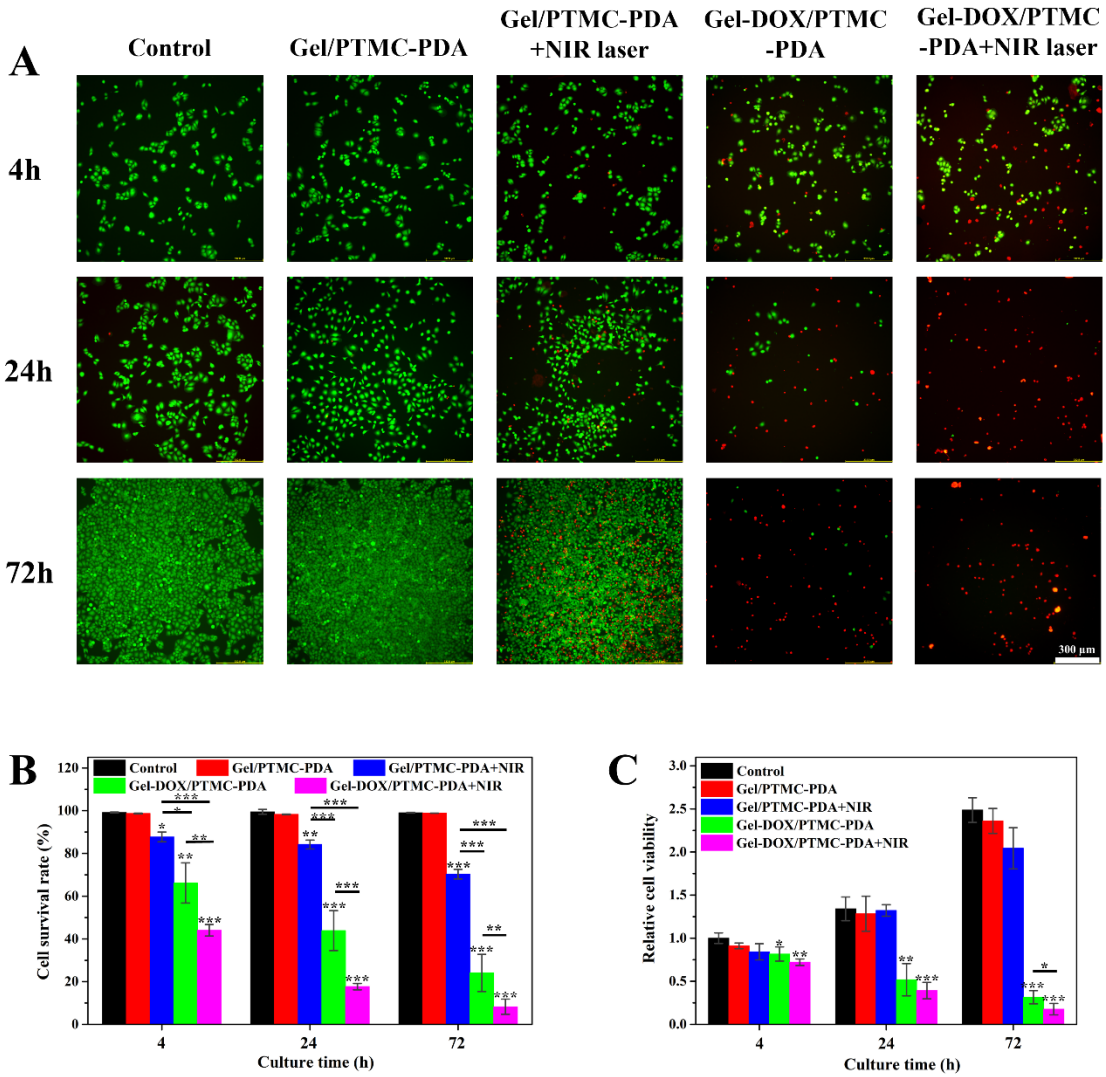

Fig.8 *In vitro* antitumor efficiency of the core/shell scaffolds. (A) Fluorescence images showing live/dead staining results of Hela cells. (B) Cell survival rate and (C) MTT results of Hela cells.

3.7 *In vitro* biological evaluation of the core/shell scaffolds

Many studied have demonstrated the efficacy and safety of BMSCs on uterine regeneration *in vitro* and *in vivo* [72, 73]. For example, Ji *et al.* fabricated a human induced pluripotent stem cell-derived mesenchymal stem cell (hiMSC)-loaded hydrogel scaffold via 3D bioprinting for repair of uterine endometrium injury [74]. They found that 3D-printed hiMSC-loaded hydrogels could facilitate the recovery of the endometrial histomorphology (endometrial tissue and gland regeneration) and endometrial cells (stromal cells and epithelial cells) and endothelial cells proliferation, and meanwhile promote endometrial receptivity functional indicators. Therefore, in the

current study, BMSCs were used to evaluate the *in vitro* biological performance of core/shell scaffolds. The live/dead assay results in Fig.9A indicated that BMSCs cultured on PTMC, Gel/PTMC, Gel/PTMC-PDA, and Gel/PTMC-PDA@E2 scaffolds exhibited well-spread morphology, suggesting that the core/shell scaffolds are biocompatible. Notably, after cultured for 4h, BMSCs on PTMC and Gel/PTMC scaffolds exhibited spherical morphology while cells began to extend and showed spindle morphology on Gel/PTMC-PDA and Gel/PTMC-PDA@E2 scaffolds. This might be attributed to the function of PDA particles and E2 biomolecule. Moreover, as shown in Fig.9B, the cell survival rate of BMSCs on all scaffolds were over 90% after cultured for 4, 24, and 48h, respectively. The proliferation behavior of the core/shell scaffolds was conducted via MTT test. Compared to PTMC and Gel/PTMC scaffolds, Gel/PTMC-PDA and Gel/PTMC-PDA@E2 scaffolds had higher cell proliferation rate (Fig.9C). Many studies have revealed that PDA particles could improve scaffolds surface wettability and scaffold-cell interface behavior and thus bolster cell growth [75, 76]. Also, due to the continuous release of E2, Gel/PTMC-PDA@E2 scaffold exhibited the highest BMSCs proliferation rate, which was consistent with previous studies [34, 77]. Further phalloidin/DAPI staining results in Fig.9D displayed that BMSCs cultured on PTMC and Gel/PTMC scaffolds, Gel/PTMC-PDA, and Gel/PTMC-PDA@E2 scaffolds were well-spread and maintained their phenotypes. As a result, the core/shell scaffolds were significantly biocompatible and could promote cell growth.

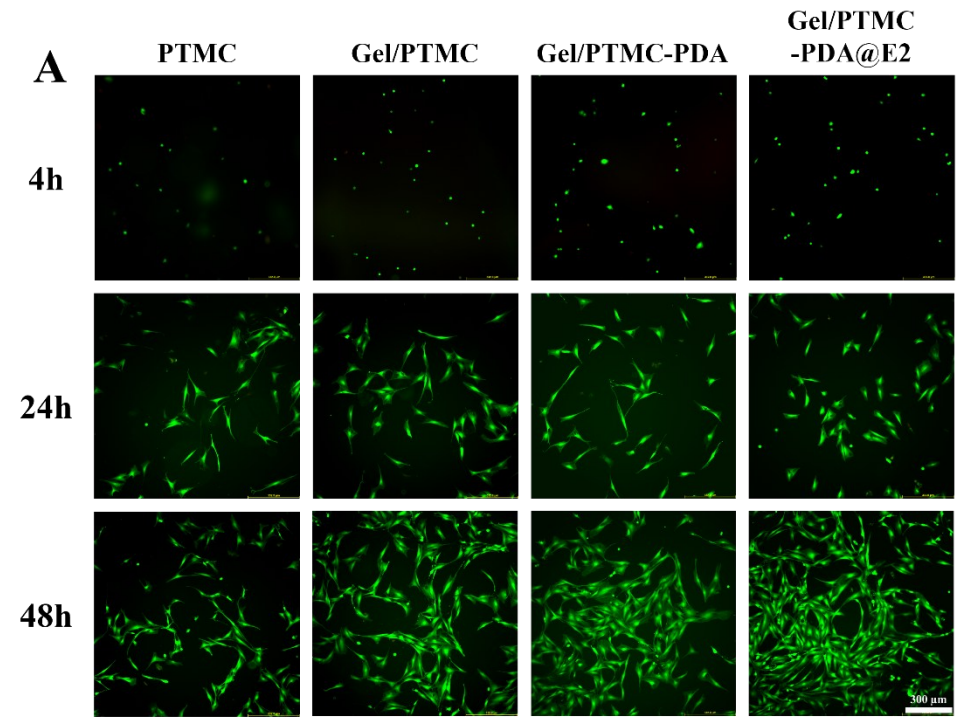
A
PTMC
Gel/PTMC
Gel/PTMC-PDA
Gel/PTMC
-PDA@E2
4h
24h
48h
300 μm

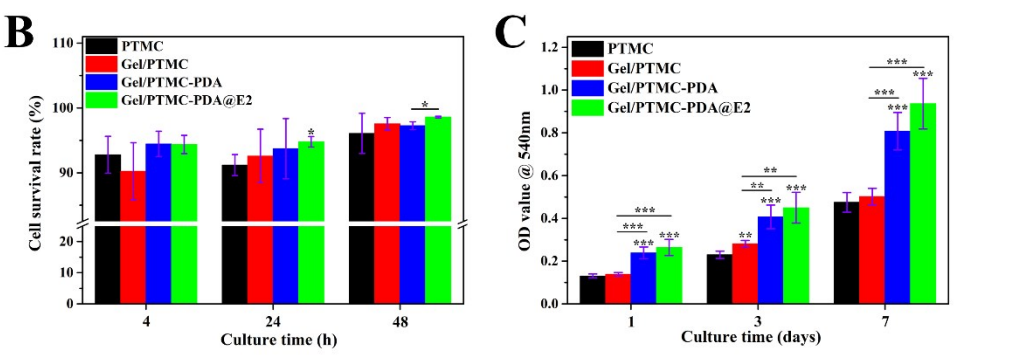
B
PTMC
Gel/PTMC
Gel/PTMC-PDA
Gel/PTMC-PDA@E2
Cell survival rate (%)
Culture time (h)
C
OD value @ 540nm
Culture time (days)

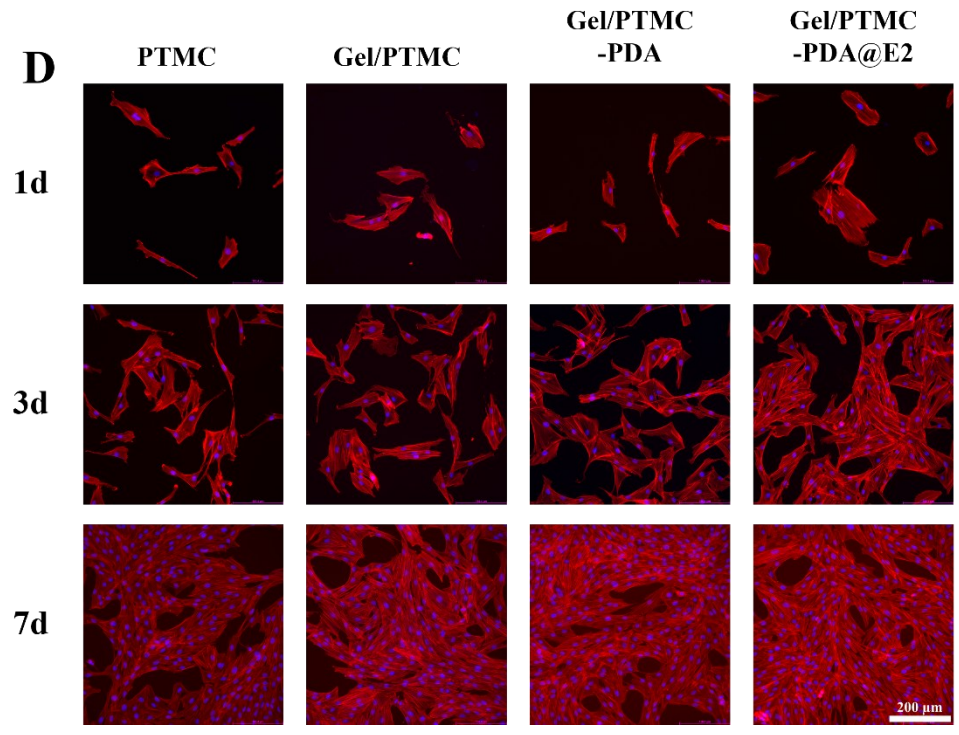
D
PTMC
Gel/PTMC
Gel/PTMC
-PDA
Gel/PTMC
-PDA@E2
1d
3d
7d
200 μm

Fig.9 *In vitro* biological performance of the core/shell scaffolds. (A) Fluorescence images of live/dead assay and (B) cell survival rates of BMSCs cultured on PTMC, Gel/PTMC, Gel/PTMC-PDA, and Gel/PTMC-PDA@E2 scaffolds for 4, 24, and 48h. (C) Proliferation behavior and (D) confocal images showing the morphology of BMSCs cultured on PTMC, Gel/PTMC, Gel/PTMC-PDA, and Gel/PTMC-PDA@E2 scaffolds for 1, 3, and 7 days.

4 Conclusions

In this study, novel multifunctional 3D printed Gel-DOX/PTMC-PDA@E2 core/shell scaffolds were successfully fabricated for cancer therapy and uterine regeneration. The coating layer significantly enhanced the mechanical properties of core/shell scaffolds, making them comparably strong to the native uterine tissues. Additionally, the coating layer protected the Gel core from rapid degradation and thus inhabited the release of DOX. As a result, Gel-DOX/PTMC-PDA@E2 core/shell scaffolds could release DOX and E2 in a chronological manner. The *in vitro* drug release results confirmed that DOX could be released in 3 days and E2 could be sustainably released over 28 days. Furthermore, the release of DOX and E2 could be precisely tuned by NIR laser irradiation. The *in vitro* antitumor test proved the synergistic effect of chemotherapy and PTT, which were provided by Gel-DOX/PTMC-PDA@E2 core/shell scaffolds, for tumor cell eradiation. Moreover, the *in vitro* biological evaluation indicated that Gel-DOX/PTMC-PDA@E2 scaffolds could promote the proliferation of BMSCs due to the continuous release of E2, which would be beneficial for uterine regeneration. Therefore, Gel-DOX/PTMC-PDA@E2 core/shell scaffolds possessing multifunction would be potential promise for cancer therapy and uterine regeneration.

Author Contributions

Shangsi Chen: Design of the research, methodology, investigation, writing and revision; **Jiahui Lai:** Methodology, investigation; **Jizhuo Chen:** Methodology, investigation; **Liwu Zheng:** writing, reviewing and editing; **Min Wang:** Design of the research, research supervision, writing, reviewing and editing and revision.

Conflicts of interest

There are no conflicts to declare.

Acknowledgments

M. Wang thanks Hong Kong's Research Grants Council (RGC) for the financial support for this work through research grants 17200519, 17202921, 17201622 and N_HKU749/22 and also The University of Hong Kong (HKU) through research grants in its Seed Fund for Basic Research Scheme. S. Chen thanks HKU for providing him with a PhD scholarship. Assistance provided by members of M. Wang's research group and by technical staff in HKU's Department of Mechanical Engineering, Faculty of Dentistry and Electron Microscopy Unit is acknowledged.

References

[1] M. Vander Borght, C. Wyns, Fertility and infertility: Definition and epidemiology, Clin Biochem 62 (2018) 2-10.
[2] F. Zegers-Hochschild, G.D. Adamson, J. de Mouzon, O. Ishihara, R. Mansour, K. Nygren, E. Sullivan, S. van der Poel, The international committee for monitoring assisted reproductive technology (ICMART) and the World Health Organization (WHO) revised glossary on ART terminology, 2009, Hum Reprod 24(11) (2009) 2683-2687.
[3] L. Chen, L. Li, Q. Mo, X. Zhang, C. Chen, Y. Wu, X. Zeng, K. Deng, N. Liu, P. Zhu, M. Liu, Y. Xiao, An injectable gelatin/sericin hydrogel loaded with human umbilical cord mesenchymal stem cells for the treatment of uterine injury, Bioeng Transl Med 8(1) (2023) e10328.
[4] N. Noyes, J.M. Knopman, K. Long, J.M. Coletta, N.R. Abu-Rustum, Fertility considerations in the management of gynecologic malignancies, Gynecol Oncol 120(3) (2011) 326-33.
[5] G.S. Sohn, S. Cho, Y.M. Kim, C.H. Cho, M.R. Kim, S.R. Lee, Current medical treatment of uterine fibroids, Obstet Gynecol Sci 61(2) (2018) 192-201.
[6] K.A. So, S.H. Shim, S.J. Lee, T.J. Kim, Surgical treatment outcomes of gynecologic sancer in older patients: A retrospective study, J Clin Med 12(7) (2023) 2518.
[7] M. Song, M.N. Kumaran, M. Gounder, D.G. Gibbon, W. Nieves-Neira, A. Vaidya, M. Hellmann, M.P. Kane, B. Buckley, W. Shih, P.B. Caffrey, G.D. Frenkel, L. Rodriguez-Rodriguez, Phase I trial of selenium plus chemotherapy in gynecologic cancers, Gynecol Oncol 150(3) (2018) 478-486.
[8] B.E. Amendola, A. Mahadevan, J.M. Blanco Suarez, R.J. Griffin, X. Wu, N.C. Perez, D.S. Hippe, C.B. Simone, 2nd, M. Mohiuddin, M. Mohiuddin, J.W. Snider, H. Zhang, Q.T. Le, N.A. Mayr, An international sonsensus on the design of prospective clinical-translational trials in spatially fractionated radiation therapy for advanced gynecologic cancer, Cancers 14(17) (2022) 4267.
[9] A. Al-Hendy, L. Bradley, C.D. Owens, H. Wang, K.T. Barnhart, E. Feinberg, W.D. Schlaff, E.E. Puscheck, A. Wang, V. Gillispie, S. Hurtado, O. Muneyyirci-Delale, D.F. Archer, B.R. Carr, J.A. Simon, E.A. Stewart, Predictors of response for elagolix with add-back therapy in women with heavy menstrual bleeding associated with uterine fibroids, Am J Obstet Gynecol 224(1) (2021) 72 e1-72 e50.
[10] S. Mitra, M.S. Lami, A. Ghosh, R. Das, T.E. Tallei, Fatimawali, F. Islam, K. Dhama, M.Y. Begum, A. Aldahish, K. Chidambaram, T.B. Emran, Hormonal therapy for gynecological sancers: How far has science progressed toward clinical applications?, Cancers 14(3) (2022) 759.
[11] Y. Luo, X. Wei, Y. Wan, X. Lin, Z. Wang, P. Huang, 3D printing of hydrogel scaffolds for future application in photothermal therapy of breast cancer and tissue repair, Acta Biomater 92 (2019) 37-47.
[12] X. Zhang, H. Wei, C. Dong, J. Wang, T. Zhang, L. Huang, D. Ni, Y. Luo, 3D printed hydrogel/bioceramics core/shell scaffold with NIR-II triggered drug release for chemo-photothermal therapy of bone tumors and enhanced bone repair, Chem Eng J 461 (2023).
[13] C. He, L. Yu, H. Yao, Y. Chen, Y. Hao, Combinatorial photothermal 3D‐printing scaffold and checkpoint blockade inhibits growth/metastasis of breast cancer to bone and accelerates osteogenesis, Adv Funct Mater 31(10) (2020).

[14] S. Chen, Y. Wang, X. Zhang, J. Ma, M. Wang, Double-crosslinked bifunctional hydrogels with encapsulated anti-cancer drug for bone tumor cell ablation and bone tissue regeneration, Colloids Surf B Biointerfaces 213 (2022) 112364.
[15] A.I. Rezk, J. Lee, B.S. Kim, S. Chun, Strategically designed bifunctional polydopamine enwrapping polycaprolactone-hydroxyapatite-doxorubicin composite nanofibers for osteosarcoma treatment and bone regeneration, ACS Appl Mater Interfaces (2024).
[16] W. He, C. Li, S. Zhao, Z. Li, J. Wu, J. Li, H. Zhou, Y. Yang, Y. Xu, H. Xia, Integrating coaxial electrospinning and 3D printing technologies for the development of biphasic porous scaffolds enabling spatiotemporal control in tumor ablation and osteochondral regeneration, Bioact Mater 34 (2024) 338-353.
[17] L. Zhao, J. Xu, Y. Tong, P. Gong, F. Gao, H. Li, Y. Jiang, Injectable "cocktail" hydrogel with dual-stimuli-responsive drug release, photothermal ablation, and drug-antibody synergistic effect, SmartMat 5(2) (2024) e1148.
[18] K. Peng, L. Zheng, T. Zhou, C. Zhang, H. Li, Light manipulation for fabrication of hydrogels and their biological applications, Acta Biomater 137 (2022) 20-43.
[19] S.Q. Wang, Y. Wang, X. Yang, Y. Liu, H. Li, Z. Yang, W.Y. Sun, J.L. Sessler, High-nuclearity luminescent lanthanide nanocages for tumor drug delivery, Angew Chem Int Ed Engl 63(12) (2024) e202317775.
[20] T.P. Ribeiro, M. Flores, S. Madureira, F. Zanotto, F.J. Monteiro, M.S. Laranjeira, Magnetic bone tissue engineering: Reviewing the effects of magnetic stimulation on bone regeneration and angiogenesis, Pharmaceutics 15(4) (2023) 1045.
[21] M.A. Mofazzal Jahromi, P. Sahandi Zangabad, S.M. Moosavi Basri, K. Sahandi Zangabad, A. Ghamarypour, A.R. Aref, M. Karimi, M.R. Hamblin, Nanomedicine and advanced technologies for burns: Preventing infection and facilitating wound healing, Adv Drug Deliv Rev 123 (2018) 33-64.
[22] Z. Wan, P. Zhang, L. Lv, Y. Zhou, NIR light-assisted phototherapies for bone-related diseases and bone tissue regeneration: A systematic review, Theranostics 10(25) (2020) 11837-11861.
[23] Y. Liu, T. Li, H. Ma, D. Zhai, C. Deng, J. Wang, S. Zhuo, J. Chang, C. Wu, 3D-printed scaffolds with bioactive elements-induced photothermal effect for bone tumor therapy, Acta Biomater 73 (2018) 531-546.
[24] C. Liu, Z. Wang, X. Wei, B. Chen, Y. Luo, 3D printed hydrogel/PCL core/shell fiber scaffolds with NIR-triggered drug release for cancer therapy and wound healing, Acta Biomater 131 (2021) 314-325.
[25] S. Chen, Y. Wang, J. Li, H. Sun, M.F.F. Siu, S. Tan, 3D-printed Mg-substituted hydroxyapatite/ gelatin methacryloyl hydrogels encapsulated with PDA@DOX particles for bone tumor therapy and bone tissue regeneration, Int J Bioprinting (2024).
[26] Y. Li, W. Hong, H. Zhang, T.T. Zhang, Z. Chen, S. Yuan, P. Peng, M. Xiao, L. Xu, Photothermally triggered cytosolic drug delivery of glucose functionalized polydopamine nanoparticles in response to tumor microenvironment for the GLUT1-targeting chemo-phototherapy, J Control Release 317 (2020) 232-245.
[27] Z. Wan, Q. Dong, Y. Liu, X. Zhang, P. Zhang, L. Lv, Y. Zhou, Programmed biomolecule delivery orchestrate bone tissue regeneration via MSC recruitment and epigenetic modulation, Chem Eng J 438 (2022).
[28] S.S. Zhang, X.X. Xu, W.W. Xiang, H.H. Zhang, H.L. Lin, L.E. Shen, Q. Lin, F. Lin, Z.Y. Zhou, Using 17beta-estradiol heparin-poloxamer thermosensitive hydrogel to enhance the endometrial regeneration and functional recovery of intrauterine adhesions in a rat model, FASEB J 34(1) (2020) 446-457.

[29] S. Chen, S. Tan, L. Zheng, M. Wang, Multilayered shape-morphing scaffolds with a hierarchical structure for uterine tissue regeneration, ACS Appl Mater Interfaces 16(6) (2024) 6772-6788.
[30] S.S. Chen, J.Z. Li, L.W. Zheng, J. Huang, M. Wang, Biomimicking trilayer scaffolds with controlled estradiol release for uterine tissue regeneration, Exploration (2024).
[31] R. Batul, M. Bhave, J.M. P, A. Yu, Polydopamine nanosphere with in-situ loaded gentamicin and its antimicrobial activity, Molecules 25(9) (2020).
[32] Y. Liu, K. Ai, J. Liu, M. Deng, Y. He, L. Lu, Dopamine-melanin colloidal nanospheres: an efficient near-infrared photothermal therapeutic agent for in vivo cancer therapy, Adv Mater 25(9) (2013) 1353-1359.
[33] Y. Wang, B. Ma, A. Yin, B. Zhang, R. Luo, J. Pan, Y. Wang, Polycaprolactone vascular graft with epigallocatechin gallate embedded sandwiched layer-by-layer functionalization for enhanced antithrombogenicity and anti-inflammation, J Control Release 320 (2020) 226-238.
[34] Y. Chen, W. Fei, Y. Zhao, F. Wang, X. Zheng, X. Luan, C. Zheng, Sustained delivery of 17beta-estradiol by human amniotic extracellular matrix (HAECM) scaffold integrated with PLGA microspheres for endometrium regeneration, Drug Deliv 27(1) (2020) 1165-1175.
[35] B. Li, L. Zhang, Y. Xie, L. Lei, W. Qu, L. Sui, Evaluation of pharmacokinetics and safety of a long-term estradiol-releasing stent in rat uterine, Regen Ther 21 (2022) 494-501.
[36] L. Xu, X. Wang, Y. Liu, G. Yang, R.J. Falconer, C.X. Zhao, Lipid nanoparticles for drug delivery, Adv Nanobiomed Res 2(2) (2021).
[37] M. Vallet-Regi, F. Schuth, D. Lozano, M. Colilla, M. Manzano, Engineering mesoporous silica nanoparticles for drug delivery: where are we after two decades?, Chem Soc Rev 51(13) (2022) 5365-5451.
[38] J. Zhang, Y. Lin, Z. Lin, Q. Wei, J. Qian, R. Ruan, X. Jiang, L. Hou, J. Song, J. Ding, H. Yang, Stimuli-responsive nanoparticles for controlled drug delivery in synergistic cancer immunotherapy, Adv Sci 9(5) (2022) e2103444.
[39] T. Bedhiafi, S. Idoudi, A.A. Alhams, Q. Fernandes, H. Iqbal, R. Basineni, S. Uddin, S. Dermime, M. Merhi, N. Billa, Applications of polydopaminic nanomaterials in mucosal drug delivery, J Control Release 353 (2023) 842-849.
[40] W. Zhong, K.H. Wong, F. Xu, N. Zhao, M. Chen, NIR-responsive polydopamine-based calcium carbonate hybrid nanoparticles delivering artesunate for cancer chemo-photothermal therapy, Acta Biomater 145 (2022) 135-145.
[41] Z. Wang, Y. Duan, Y. Duan, Application of polydopamine in tumor targeted drug delivery system and its drug release behavior, J Control Release 290 (2018) 56-74.
[42] M.K. Yazdi, M. Zare, A. Khodadadi, F. Seidi, S.M. Sajadi, P. Zarrintaj, A. Arefi, M.R. Saeb, M. Mozafari, Polydopamine biomaterials for skin regeneration, ACS Biomater Sci Eng 8(6) (2022) 2196-2219.
[43] S.H. Lee, R.A. Doong, Adsorption and selective recognition of 17ß-estradiol by molecularly imprinted polymers, J Polym Res 19 (2012) 1-12.
[44] S. Abdella, F. Afinjuomo, Y. Song, R. Upton, S. Garg, Mucoadhesive buccal film of estradiol for hormonal replacement therapy: Development and in-vivo performance prediction, Pharmaceutics 14(3) (2022) 542.
[45] R. Batul, A. Yu, M. Bhave, A. Khaliq, Synthesis of polydopamine nanoparticles for drug delivery applications, Microsc Microanal 24(S1) (2018) 1758-1759.

[46] P.L. Thi, Y. Lee, D.L. Tran, T.T.H. Thi, J.I. Kang, K.M. Park, K.D. Park, In situ forming and reactive oxygen species-scavenging gelatin hydrogels for enhancing wound healing efficacy, Acta Biomater 103 (2020) 142-152.
[47] A.M. Sisso, M.O. Boit, C.A. DeForest, Self-healing injectable gelatin hydrogels for localized therapeutic cell delivery, J Biomed Mater Res A 108(5) (2020) 1112-1121.
[48] S. Chen, Y. Shi, X. Zhang, J. Ma, Evaluation of BMP-2 and VEGF loaded 3D printed hydroxyapatite composite scaffolds with enhanced osteogenic capacity in vitro and in vivo, Materials Science and Engineering: C 112 (2020) 110893.
[49] A. Serafin, M. Culebras, M.N. Collins, Synthesis and evaluation of alginate, gelatin, and hyaluronic acid hybrid hydrogels for tissue engineering applications, Int J Biol Macromol 233 (2023) 123438.
[50] R. Rodríguez-Rodríguez, H. Espinosa-Andrews, C. Velasquillo-Martínez, Z.Y. García-Carvajal, Composite hydrogels based on gelatin, chitosan and polyvinyl alcohol to biomedical applications: a review, Int J Polym Mater Polym Biomater 69(1) (2019) 1-20.
[51] S. Chen, Y. Wang, J. Lai, S. Tan, M. Wang, Structure and properties of gelatin methacryloyl (GelMA) synthesized in different reaction systems, Biomacromolecules 24(6) (2023) 2928-2941.
[52] L.J. Ji, K.L. Lai, B. He, G. Wang, L.Q. Song, Y. Wu, Z.W. Gu, Study on poly(L-lactide-co-trimethylene carbonate): synthesis and cell compatibility of electrospun film, Biomed Mater 5(4) (2010) 045009.
[53] A. Baah-Dwomoh, J. McGuire, T. Tan, R. De Vita, Mechanical properties of female reproductive organs and supporting connective tissues: A review of the current state of knowledge, Appl Mech Rev 68(6) (2016).
[54] S.J. Manoogian, J.A. Bisplinghoff, A.R. Kemper, S.M. Duma, Dynamic material properties of the pregnant human uterus, J Biomech 45(9) (2012) 1724-7.
[55] E.G. Santoso, K. Yoshida, Y. Hirota, M. Aizawa, O. Yoshino, A. Kishida, Y. Osuga, S. Saito, T. Ushida, K.S. Furukawa, Application of detergents or high hydrostatic pressure as decellularization processes in uterine tissues and their subsequent effects on in vivo uterine regeneration in murine models, PLoS one 9(7) (2014) e103201.
[56] Q. Yao, Y.W. Zheng, H.L. Lin, Q.H. Lan, Z.W. Huang, L.F. Wang, R. Chen, J. Xiao, L. Kou, H.L. Xu, Y.Z. Zhao, Exploiting crosslinked decellularized matrix to achieve uterus regeneration and construction, Artif Cells Nanomed Biotechnol 48(1) (2020) 218-229.
[57] M. Brannstrom, Uterus transplantation and beyond, J Mater Sci Mater Med 28(5) (2017) 70.
[58] E. Chiani, A. Beaucamp, Y. Hamzeh, M. Azadfallah, A.V. Thanusha, M.N. Collins, Synthesis and characterization of gelatin/lignin hydrogels as quick release drug carriers for Ribavirin, Int J Biol Macromol 224 (2023) 1196-1205.
[59] S.S. Chen, Y.F. Shi, X. Zhang, J. Ma, Evaluation of BMP-2 and VEGF loaded 3D printed hydroxyapatite composite scaffolds with enhanced osteogenic capacity

and, Mater Sci Eng C Mater Biol Appl 112 (2020).
[60] W. Cheng, J.P. Nie, N.S. Gao, G. Liu, W. Tao, X.J. Xiao, L.J. Jiang, Z.G. Liu, X.W. Zeng, L. Mei, A multifunctional nanoplatform against multidrug resistant cancer: Merging the best of targeted chemo/gene/photothermal therapy, Adv Funct Mater 27(45) (2017).

[61] L. Ning, C. You, Y. Zhang, X. Li, F. Wang, Polydopamine loaded fluorescent nanocellulose–agarose hydrogel: A pH-responsive drug delivery carrier for cancer therapy, Compos Commun 26 (2021).
[62] H. Li, Y. Jia, X. Feng, J. Li, Facile fabrication of robust polydopamine microcapsules for insulin delivery, J Colloid Interface Sci 487 (2017) 12-19.
[63] L. Xu, K. Crawford, C.B. Gorman, Effects of temperature and pH on the degradation of poly(lactic acid) brushes, Macromolecules 44(12) (2011) 4777-4782.
[64] F. Qu, J.L. Holloway, J.L. Esterhai, J.A. Burdick, R.L. Mauck, Programmed biomolecule delivery to enable and direct cell migration for connective tissue repair, Nat Commun 8(1) (2017) 1780.
[65] L.S. Carasso, I. Benhar, T. Dvir, Universal biofactor-releasing scaffold enabling in vivo reloading, Nano letters 19(3) (2019) 1838-1843.
[66] J. Johary, M. Xue, X. Zhu, D. Xu, P.P. Velu, Efficacy of estrogen therapy in patients with intrauterine adhesions: systematic review, J Minim Invasive Gynecol 21(1) (2014) 44-54.
[67] X. Liu, C. Wang, X. Wang, C. Tian, Y. Shen, M. Zhu, A dual-targeting Fe(3)O(4)@C/ZnO-DOX-FA nanoplatform with pH-responsive drug release and synergetic chemo-photothermal antitumor in vitro and in vivo, Mater Sci Eng C Mater Biol Appl 118 (2021) 111455.
[68] M.H. Hsieh, T.H. Wang, S.H. Hu, T.C. Hsu, J.L. Yow, B.S. Tzang, W.H. Chiang, Tumor site-specific PEG detachment and active tumor homing of therapeutic PEGylated chitosan/folate-decorated polydopamine nanoparticles to augment antitumor efficacy of photothermal/chemo combination therapy, Chem Eng J 446 (2022).
[69] M. Gulfam, S.H. Jo, S.W. Jo, T.T. Vu, S.H. Park, K.T. Lim, Highly porous and injectable hydrogels derived from cartilage acellularized matrix exhibit reduction and NIR light dual-responsive drug release properties for application in antitumor therapy, Npg Asia Mater 14(1) (2022) 8.
[70] Z. Wang, H. Cheng, Y. Sheng, Z. Chen, X. Zhu, J. Ren, X. Zhang, L. Lv, H. Zhang, J. Zhou, Y. Ding, Biofunctionalized graphene oxide nanosheet for amplifying antitumor therapy: Multimodal high drug encapsulation, prolonged hyperthermal window, and deep-site burst drug release, Biomaterials 287 (2022) 121629.
[71] L. Zhang, X. Guan, X. Xiao, Y. Chai, Z. Chen, G. Zhou, Y. Fan, Near-infrared triggered injectable ferrimagnetic chitosan thermosensitive hydrogel for photo hyperthermia and precisely controlled drug release in tumor ablation, Eur Polym J 162 (2022).
[72] Z. Jing, Z. Qiong, W. Yonggang, L. Yanping, Rat bone marrow mesenchymal stem cells improve regeneration of thin endometrium in rat, Fertil Steril 101(2) (2014) 587-94.
[73] L. Gao, Z. Huang, H. Lin, Y. Tian, P. Li, S. Lin, Bone marrow mesenchymal stem cells (BMSCs) restore functional endometrium in the rat model for severe asherman syndrome, Reprod Sci 26(3) (2019) 436-444.
[74] W. Ji, B. Hou, W. Lin, L. Wang, W. Zheng, W. Li, J. Zheng, X. Wen, P. He, 3D Bioprinting a human iPSC-derived MSC-loaded scaffold for repair of the uterine endometrium, Acta Biomater 116 (2020) 268-284.
[75] I. Cruz-Maya, S. Zuppolini, M. Zarrelli, E. Mazzotta, A. Borriello, C. Malitesta, V. Guarino, Polydopamine-coated alginate microgels: Process optimization and in vitro validation, J Funct Biomater 14(1) (2022) 2.

[76] S. Fan, Y. Wan, Z. Zhao, H. Wang, Z. Ji, Biological evaluation of polydopamine and chitosan composite coatings on the 3D printed porous biphasic calcium phosphate scaffold, Ceram Int 48(19) (2022) 27942-27956.
[77] Q. Yao, Y.W. Zheng, Q.H. Lan, L.F. Wang, Z.W. Huang, R. Chen, Y. Yang, H.L. Xu, L. Kou, Y.Z. Zhao, Aloe/poloxamer hydrogel as an injectable beta-estradiol delivery scaffold with multi-therapeutic effects to promote endometrial regeneration for intrauterine adhesion treatment, Eur J Pharm Sci 148 (2020) 105316.

Supporting Information

3D Printed Gelatin/PTMC Core/Shell Scaffolds with NIR Laser-Tuned Drug/Biomolecule Release for Cancer Therapy and Uterine Regeneration

Shangsi Chen [a], Jiahui Lai [a], Jizhuo Chen [a], Liwu Zheng [b], Min Wang [a, *]

[a] Department of Mechanical Engineering

The University of Hong Kong

Pokfulam Road, Hong Kong SAR, China

[b] Faculty of Dentistry

The University of Hong Kong

34 Hospital Road, Sai Ying Pun, Hong Kong SAR, China

Keywords: 3D printing, core/shell scaffolds, cancer therapy, uterine regeneration, dual release

* Corresponding Author:

Professor Min Wang, at the University of Hong Kong, Hong Kong, China

Email: memwang@hku.hk Tel: +852 3971 7903 Fax: +852 2858541

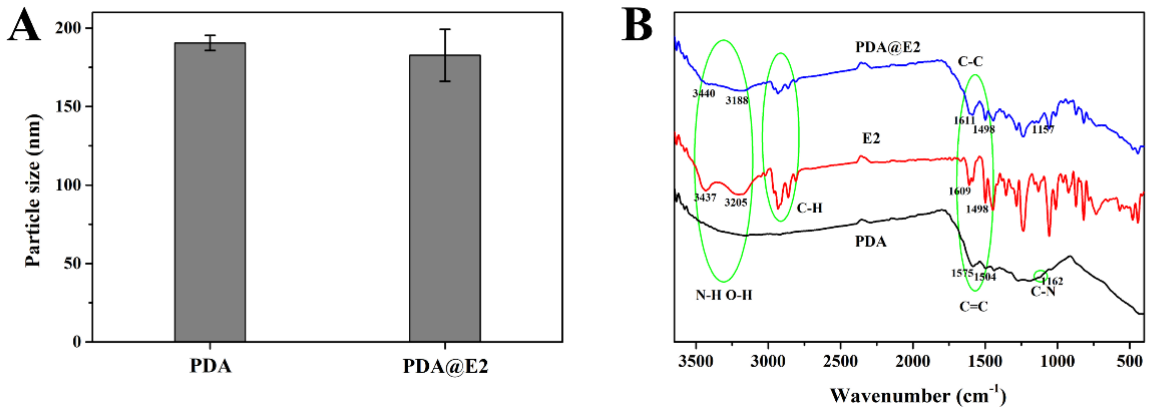

Fig.S1 (A) PDA and PDA@E2 particle size. (B) FT-IR spectra of PDA, E2, and PDA@E2.

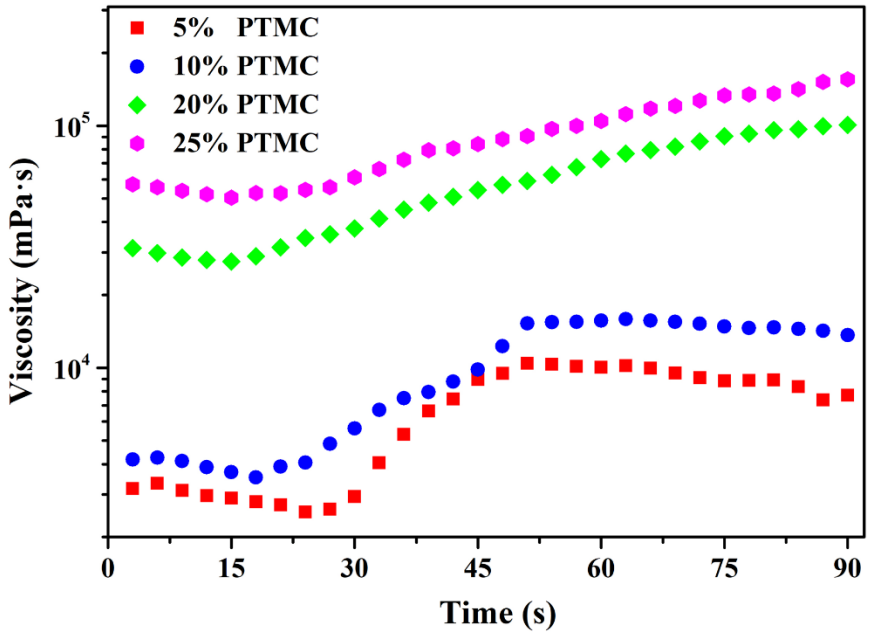

Fig.S2 The viscosity of different concentrations (5, 10, 20, and 25%) of PTMC solutions.

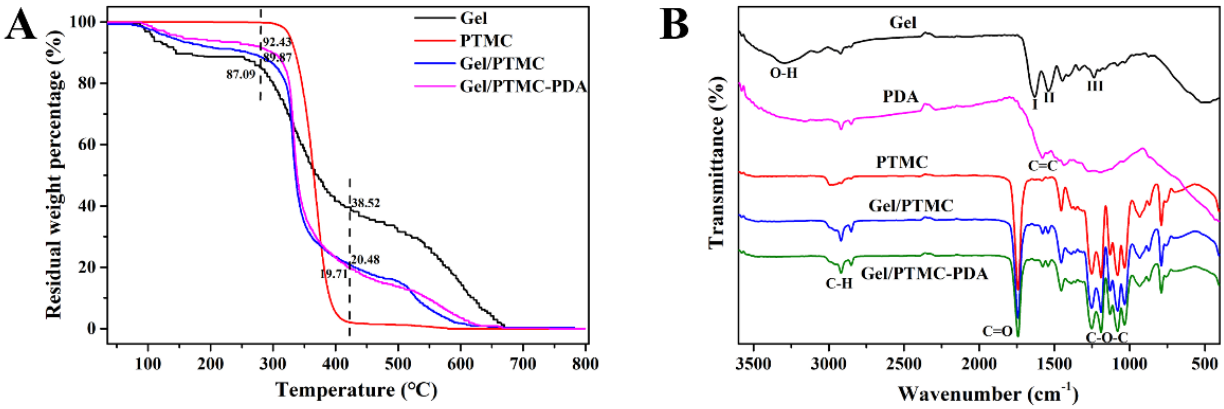

Fig.S3 (A) TGA results of Gel, PTMC, Gel/PTMC, and Gel/PTMC-PDA scaffolds. (B) FT-IR spectra of Gel, PDA, PTMC, Gel/PTMC, and Gel/PTMC-PDA.

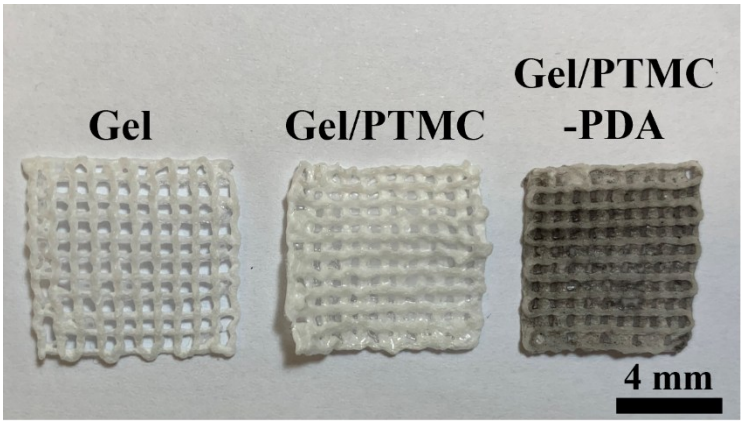

Fig.S4 The macroscopic photo of Gel, Gel/PTMC, and Gel/PTMC-PDA scaffolds.

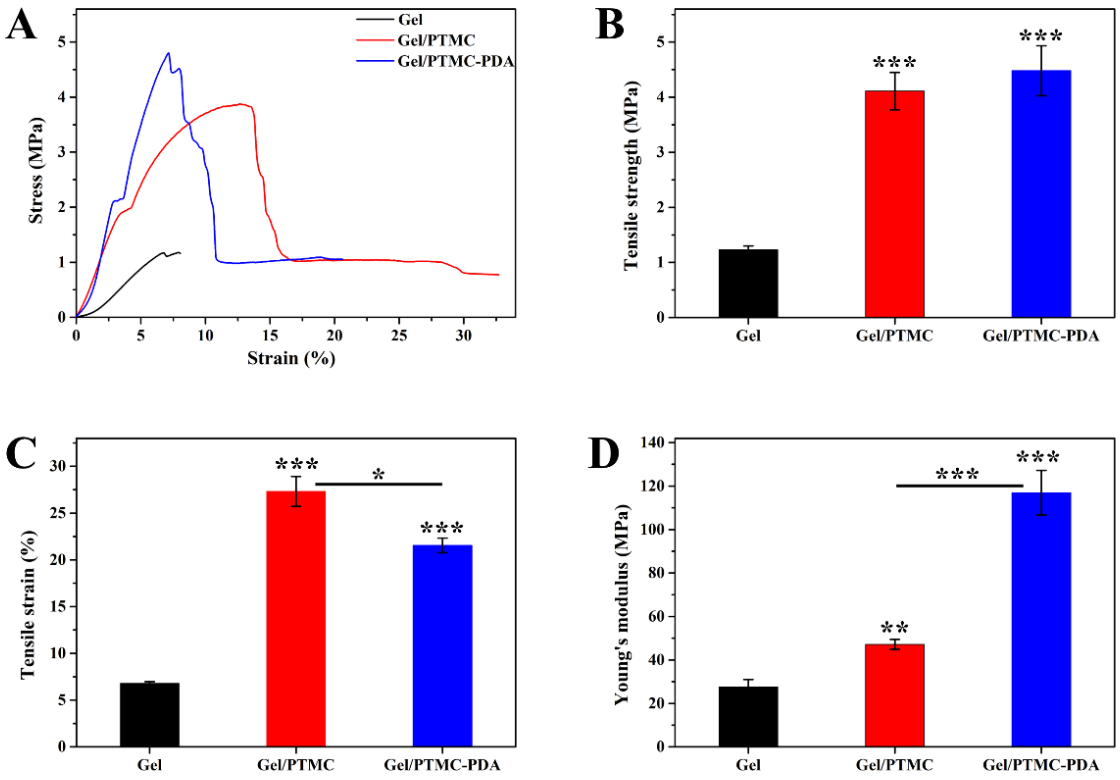

Fig.S5 The mechanical properties of dried Gel, Gel/PTMC, and Gel/PTMC-PDA scaffolds. (A) Stress-strain curves, (B) tensile strength, (C) tensile strain and (D) Young's modulus of Gel, Gel/PTMC, and Gel/PTMC-PDA scaffolds.

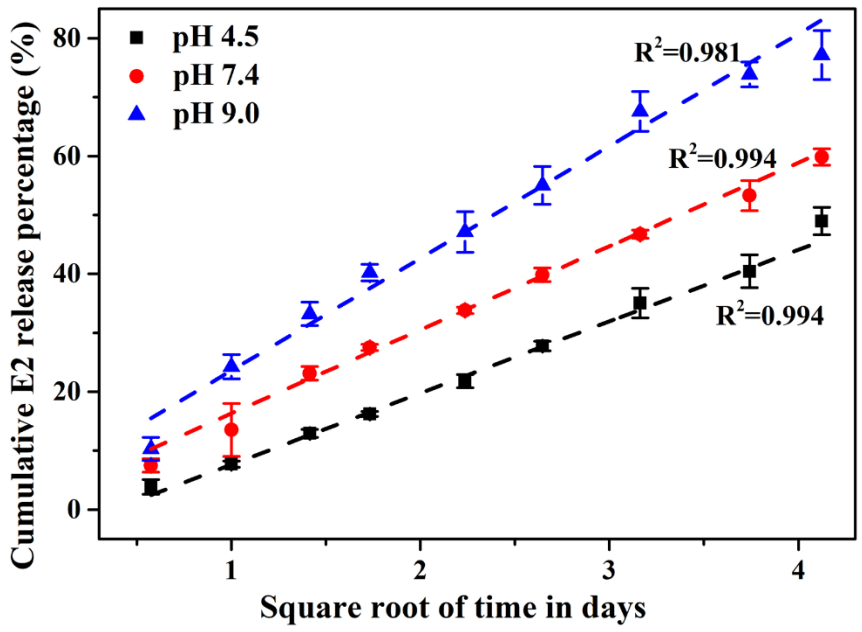

Fig.S6 The Higuchi model of E2 release kinetics of Gel/PTMC-PDA@E2 scaffolds in pH 4.5, 7.4, and 9.0 buffer solutions.